KERNFORSCHUNGSANLAGE JÜLICH GmbH
Institut für Festkörperforschung

ATOMIC DISPLACEMENT RATES OF LIGHT IONS IN CUBIC METALS

by

Peter Jung

Jül - 1823
Januar 1983
ISSN 0366 - 0885

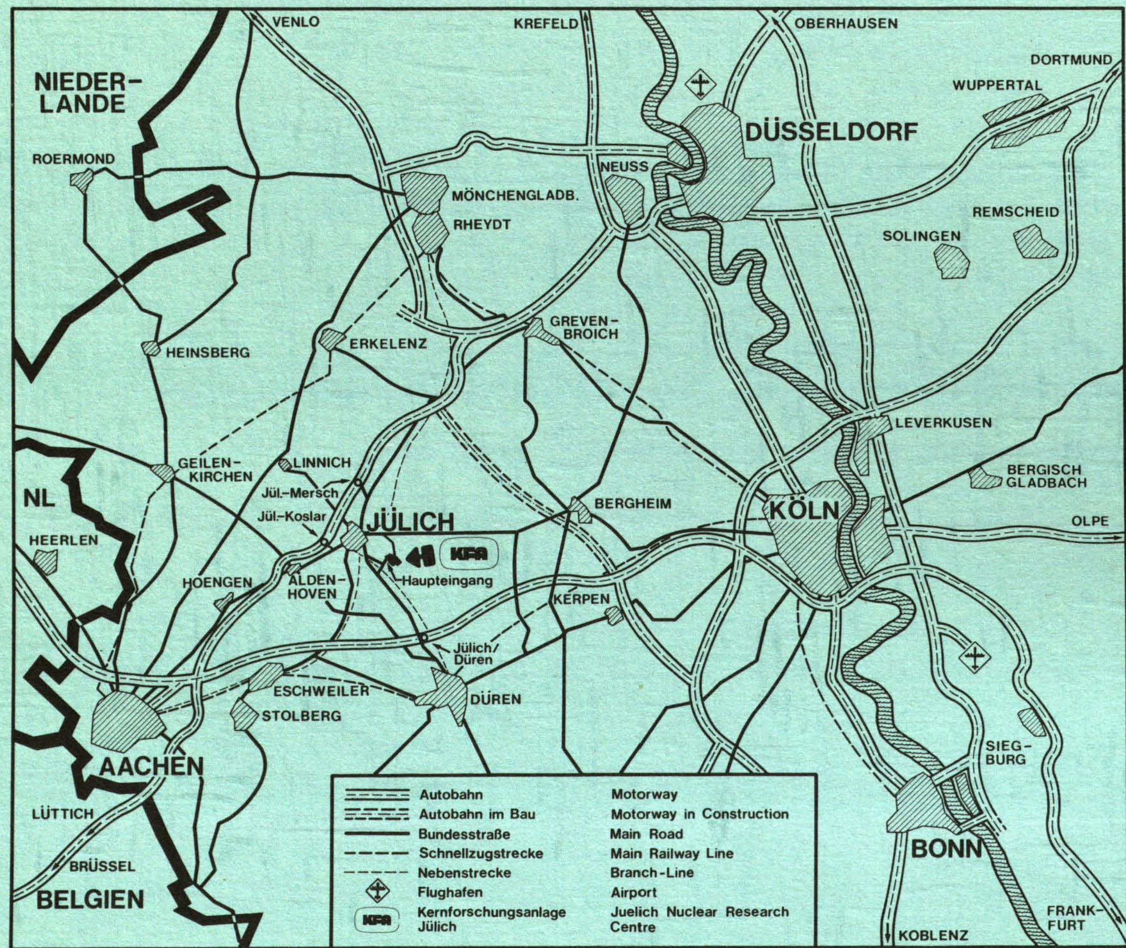

Als Manuskript gedruckt

Berichte der Kernforschungsanlage Jülich - Nr. 1823

Institut für Festkörperforschung Jül - 1823

Zu beziehen durch: ZENTRALBIBLIOTHEK der Kernforschungsanlage Jülich GmbH
Postfach 1913 · D-5170 Jülich (Bundesrepublik Deutschland)
Telefon: (0 24 61) 610 · Telex: 8 33 556 kfa d

ATOMIC DISPLACEMENT RATES OF LIGHT IONS IN CUBIC METALS

by

Peter Jung

Institut für Festkörperforschung der
Kernforschungsanlage Jülich GmbH,
D-5170 Jülich, West Germany,
Assoziation Euratom-KFA.

A B S T R A C T

Atomic displacement rates of light ions in cubic metals (Al, V, Fe, Cu, Nb, Mo, Ag, Pt and Au) are calculated. The parameters used are chosen such that the calculations fit all available data of electron, ion and fast neutron irradiations as closely as possible. This procedure allows a more reliable extension of the calculations to energies beyond the range of existing data. Interpolation of the parameters of different materials enables the calculation of displacement rates for metals where no light ion data are available, (Ni, Pd, Ta, W and stainless steel). Furtheron helium-to-dpa ratios are calculated for those metals, which are of interest for fusion reactor applications.

The displacement cross sections, helium-to-dpa ratios and numbers of defects produced during α-implantation derived in this work are considered the best presently available and are recommended for dpa-calculations in light-ion simulation experiments.

I. Introduction

Irradiation of metals by light ions in the 10 MeV range is used to simulate mechanical property changes induced by neutrons in fast fission or future fusion reactors /1/. Data from simulation experiments can only be used for reactor design applications if the relation between the atomic displacement rates of the simulation particles and the reactor neutrons is known.

The standard technique to derive defect production rates is resistivity measurement after low temperature irradiation. The concentration of displaced atoms c_d is derived from the measured resistivity change $\Delta\rho$ by:

$$c_d = \frac{\Delta\rho}{\rho_F} \qquad (1)$$

ρ_F is the resistivity contribution per unit concentration of defects. Such measurements have been performed for most of the more common transition metals under electron /2/ and fast neutron irradiation /3/. For light ions only recently systematic measurements for a greater number of metals became available /4/. For small defect concentrations, c_d is proportional to the fluence ϕ, the ratio being the so-called displacement cross section σ_d:

$$\sigma_d = \frac{c_d}{\phi} \quad \text{or} \quad \sigma_d = \frac{1}{\rho_F} \cdot \frac{\Delta\rho}{\Delta\phi} \qquad (2)$$

where $\frac{\Delta\rho}{\Delta\phi}$ is the measured damage rate extrapolated to zero defect concentration. The total number of defects produced by a particle in a "thin" target of atomic density N_t and thickness d is then given by:

$$N_d = N_t \cdot \sigma_d \cdot d \qquad (3)$$

For calculating σ_d, the particle-target interaction where the irradiation particle transfers energy to a primary atom (PKA) is separated from the interaction of the PKA with the other lattice atoms. For monoenergetic particles σ_d is usually written as:

$$\sigma_d(E) = \int_{T_{d,min}}^{T_m(E)} \frac{d\sigma}{dT}(E,T)\,\nu(T)\,dT \qquad (4)$$

$T_{d,min}$ is the minimum atomic displacement energy (compare /2/), T_m is the maximum energy which can be transferred to the PKA by the incoming particle plus the recoil energies from possible nuclear reaction products. The differential cross section $\frac{d\sigma}{dT}$ describes the probability of a certain energy transfer T (by incoming plus outgoing particles) to the PKA. The displacement function $\nu(T)$ gives the average number of permanently displaced atoms for a PKA of energy T.

The separation between particle-PKA and PKA-lattice interaction is only reasonable as long as both interactions are clearly distinguishable. This is certainly the case for electrons, light ions and fast neutrons where the particle-PKA events are widely separated while the PKA-lattice interactions (displacement cascade) are highly concentrated around the PKA site. The separation fails when the particle mass approaches or exceeds the mass of the target atoms. In this case distances between primary events are similar to or closer than the extension of the displacement cascades. In the case of self-ion irradiation N_d is set equal to $\nu(E)$.

It is the aim of the present work to derive $\nu(T)$ functions which fit electron, light ion, self-ion and fast neutron data for those metals where sufficient data are available, i.e. Al, V, Fe, Cu, Nb, Mo, Ag, Pt, Au. The $\nu(T)$ function is then used to calculate defect production rates for proton, deuteron and α-irradiation and for α-implantation up to energies around 20 MeV. The results for α-implantation in Cu and Ag are compared to experimental data. For those metals (Ni, stainless steel, Pd, Ta and W) for which only data from electrons and neutrons are available, the $\nu(T)$ functions are estimated by interpolation and a general expression for $\nu(T)$ is given for other metals. For those of the above metals which are of special interest for fusion reactor application (Al, V, Fe, Ni, Cu, Mo) also helium production cross sections are compiled and ratios of helium production to displacement rates are calculated.

II. Differential cross section

The energy transfer from the irradiation particle to the PKA occurs by elastic and by inelastic processes. In the latter case nuclear excitation or formation of a compound nucleus takes place. If the compound nucleus is unstable it decays by emitting one or more secondary particles.

a) Electrons

Elastic collisions between charged particles are described by the Rutherford cross section. For fast electrons, relativistic and exchange corrections must be included, yielding the so-called Mott-cross section which is used in the present work in the form given by Oen /5/. Inelastic scattering is negligible in the energy range considered here.

b) Fast neutrons

Differential cross section for different fast neutron spectra (maximum energy E_{max}) for the metals under consideration are given in /3/, /6/, and /7/ in the form of an "energy-cross-section" $\langle \sigma_d T \rangle$

$$\langle \sigma_d T \rangle = \int_0^{E_{max}} \frac{d\phi}{dE}\, dE \int_{T_{d,min}}^{T_m} \cdot \frac{d\sigma}{dT} \cdot \beta \cdot \frac{T}{\eta}\, dT \qquad (5)$$

where $\frac{d\phi}{dE}$ is the fractional flux of particles per energy interval. T/η is the so-called damage energy as described in the next section and β is a numerical factor.

c) Light ions

The interaction of light ions with matter is described by the Rutherford cross section for a wide range of energies or particle-target distances. At low energy transfers, that means at large distances between ion and target nucleus, shielding by the atomic electrons occurs. Therefore, for low energy transfers, a screening correction must be applied to the Rutherford cross section. The screening has been treated by Lindhard and co-workers /8/ by using a Thomas Fermi potential. An approximate analytical expression of the resulting differential cross section has been recently derived /9/, and will be used in the present calculations:

$$\frac{d\sigma}{dT} = \pi a^2 \quad \frac{\lambda}{2Tt^{1/3}\left[1+(2\lambda t^{2/3})^{2/3}\right]^{3/2}} \qquad (6)$$

$$\lambda = 1.309$$

$$a = \frac{0.8853\ a_o}{\sqrt{z^{2/3}+Z^{2/3}}}$$

$$t = \frac{ET}{(e^2/a)^2} \cdot \frac{M}{4mz^2Z^2}$$

a_o is Bohr's radius (0.52916×10^{-8} cm). m, M, z, Z are atomic masses and numbers of the irradiation particle and target nucleus, respectively. For high values of T, equation (6) reduces to the Rutherford cross section.

At still higher T-values, that is for very close encounters of particle and target nucleus, the interaction is influenced by nuclear forces which again cause deviations from the Rutherford cross section $d\sigma_R$. The corresponding correction factor $\frac{d\sigma}{d\sigma_R}$ is known from scattering experiments. It deviates significantly from unity only for irradiation energies above the coulomb barrier E_c:

$$E_c\,[\mathrm{MeV}] \approx \frac{zZ}{m^{1/3} + M^{1/3}} \tag{7}$$

For the particle target combinations of the present work experimental $\frac{d\sigma}{d\sigma_R}$ data from /10/ (Al, V) and /11/ (Fe, Ni, Cu) are used. For the heavier elements the corrections due to nuclear interaction become negligible for energies below about 10 MeV. Fig. 1 shows some of the data for nickel. The abscissa gives the scattering angle of the particle in the center of mass system ϑ_1'. For the nonrelativistic case the following general relations hold for the scattering angle ϑ_2 of the PKA in the laboratory system and the transferred energy, respectively:

$$\vartheta_2 = \frac{1}{2}(\pi - \vartheta_1') \tag{8}$$

$$T = T_m \cos^2\vartheta_2 \tag{9}$$

$$T_m = 4E \frac{mM}{(m+M)^2} \tag{10}$$

The dashed parts of the curves in Fig. 1 are extrapolations. At small angles the cross section should approximate the Rutherford value. The curves are therefore smoothly extrapolated towards unity at small angles while at high angles only a "most-probable" type of extrapolation is possible as for high scattering angles, theoretical optical-model calculations are also rather uncertain. On the other hand, these high ϑ_1' encounters contribute so little to the total defect production that the possible error due to a wrong extrapolation would in any case be below 1 %.

In the same range of energies ($E > E_c$) where corrections of the Rutherford cross section due to nuclear forces occur, contributions due to inelastic scattering also become significant. The treatment of inelastic scattering is much more complicated than that of the elastic processes. Usually the inelastic scattering is treated as a two step process. In the first step, the irradiation particle is captured with a total cross section $\sigma_c(E)$ to form a so-called compound nucleus with kinetic energy $T_m/4$ which decays by emitting one or more particles. The decay of the 'compound' PKA is assumed to occur before its first encounter with another lattice atom.

For only one outgoing particle the transferred energy in the laboratory system is given by:

$$T = \frac{mM'}{(m+M)\ (m'+M')}\ E + \frac{m'}{M'}\ E_1' + 2\sqrt{\frac{mm'}{(m+M)\ (m'+M')}\ EE_1'}\ \cos\vartheta_1' \tag{11}$$

where m' and M' are the masses of the outgoing particle and nucleus, respectively. E_1' is the energy of the outgoing particle in the center of mass system.

For $m \ll M$, $m' \approx m$ and $M' \approx M$ equation (11) is simplified appreciably. In this approximation the range of energies (T^+ to T^-) transferred to the target nucleus is given by:

$$T^{\pm} = \frac{T_m}{4}\ \left(1 + \frac{E_1'}{E} \pm 2\sqrt{\frac{E_1'}{E}}\right) \tag{12}$$

and its scattering angle in the laboratory system is:

$$\sin\ _2 = \sqrt{\frac{m'}{M'} \cdot \frac{E_1'}{T}}\ \sin\vartheta_1' \tag{13}$$

At higher energies where inelastic processes become important, the energy distribution of an outgoing particle is approximately described by an evaporation model /12/, which in the center of mass system yields:

$$\frac{d\sigma}{dE_1'} = \sigma_c \cdot \frac{E_1'\ e^{-E_1'/\Theta}}{\Theta^2 \left[1 - (1 + E_{1,max}'/\Theta)\ e^{-E_{1,max}'/\Theta}\right]} \tag{14}$$

Θ is the temperature of the compound nucleus. E_1' ranges from zero to a maximum value:

$$E_{1,max}' = \left(1 - \frac{m'M'}{(m'+M')^2}\right) \cdot \left(E - \frac{T_m}{4} + Q\right) \approx E + Q \tag{15}$$

Q is the Q-value of the nuclear reactions. The last approximation again holds for $m \ll M$, $m' \approx m$ and $M' \approx M$.

The angular distribution of the secondary particle is fairly isotropic for small emission energies E_1', light and medium heavy elements and medium irradiation energies, and these are of interest in the present case. Only particles of high E_1' show a predominance of forward scattering /13/. As low energy emission is strongly favoured by equation (14), an isotropic distribution is assumed for elements with atomic numbers not greater than copper. For the heavier elements, again, contributions from inelastic scattering become negligible. The error resulting from neglecting nuclear interactions for the heavier elements is further reduced by the fact that the contribution of inelastic scattering to defect production is partially compensated by the prevailing lowering of the elastic cross section (Fig. 1). For an isotropic distribution the differential inelastic cross section is calculated with the aid of (12), (14) and (15) according to /14/ by:

$$\frac{d\sigma_i}{dT} = \frac{1}{T^+ - T^-} \int_0^{E'_{1,max}} \frac{d\sigma}{dE_1'} \, dE_1' \qquad (16)$$

Following /15/ and /16/ a modified version of equation (14) was used in the present work to include preequilibrium contributions:

$$\frac{d\sigma}{dE_1'} = (1-F) \frac{d\sigma}{dE_1'}/\text{equ.} + F \cdot \sigma_c \frac{12 \cdot E_1' \cdot (E-E_1')^2}{E^4} \qquad (17)$$

with $F \approx 0.1$ and $\Theta \approx 1.0$ /15/. $\frac{d\sigma}{dE_1'}$/equ. is the expression of equation (14). The integral inelastic cross section σ_i is increased by typically less than 3 % by the addition of the second term in equation (17). An increase in σ_i by about 6 % is obtained by varying Q from 0 to 4 MeV in equation (15). The largest change in σ_i is obtained by assuming zero emission energy ($E_1' = 0$) corresponding to Θ=0. But this lowers σ_i also by not more than 20 %. This also shows that the details of the treatment of the case

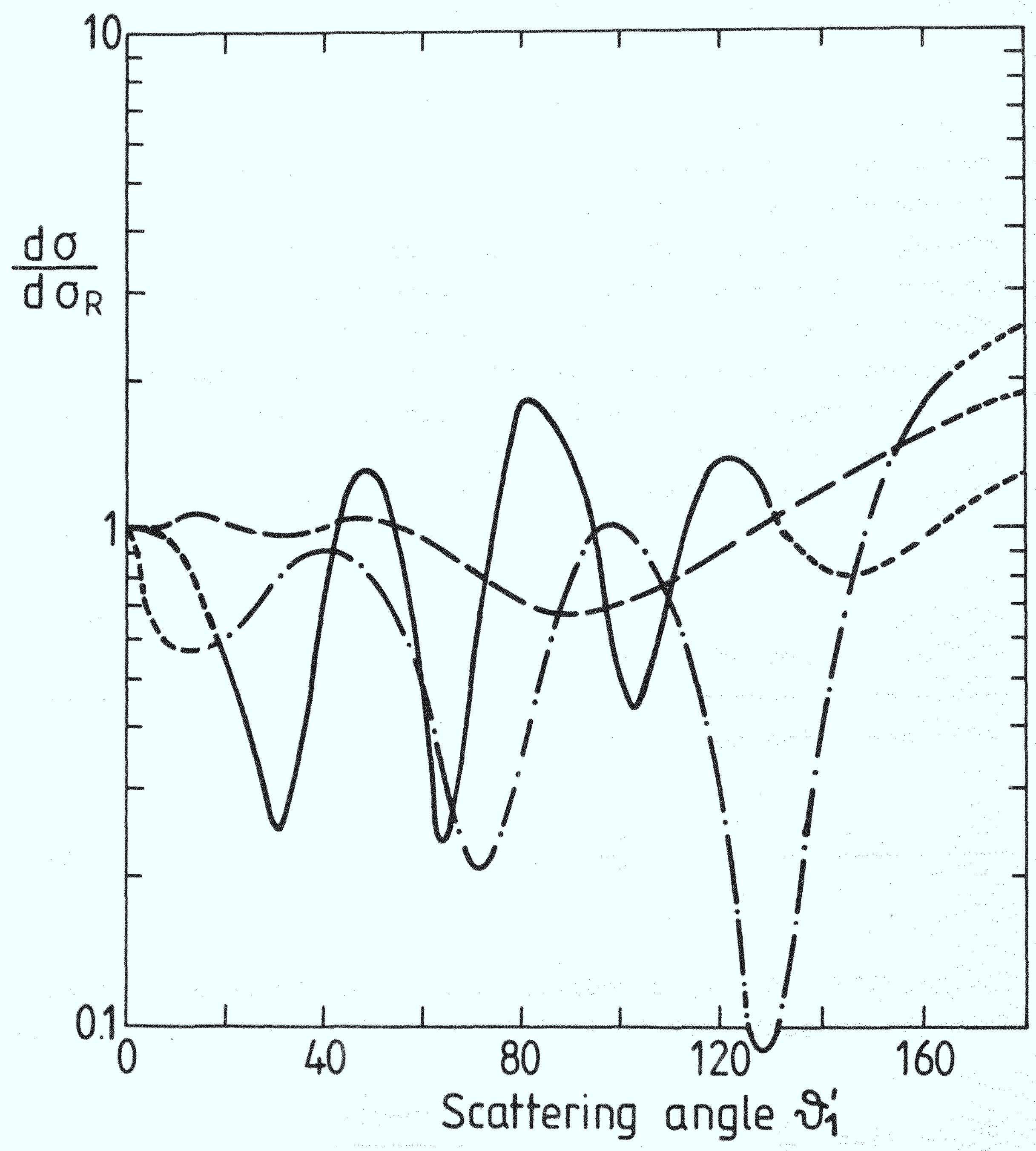

Fig. 1: Ratio of elastic scattering cross section to Rutherford cross section for protons of different energies in nickel as a function of the scattering angle in the center-of-mass system /11/. Energies are 5.25 MeV (--), 14.3 MeV (-·-) and 22.2 MeV (——). The dashed parts of the curves are extrapolated.

of more than one outgoing particle is not very important. In any case multiple emission starts to contribute only at the upper end of the energy range considered here. It was found that inelastic scattering contributes less than about 20 %

to defect production in the envisaged energy range. Therefore the total error in the calculated displacement rates caused by uncertainties in F, in Θ and in Q is expected not to exceed about 4 %. Thus in the present case the only really important parameter in equation (17) is σ_c. Since not all cross sections for all isotopes, all nuclear reactions and all energies are known, values averaged from Refs. /17-20/ for protons and from Ref. /10/ and /11/ for deuterons and α-particles were used as given in Figs. 2 to 4.

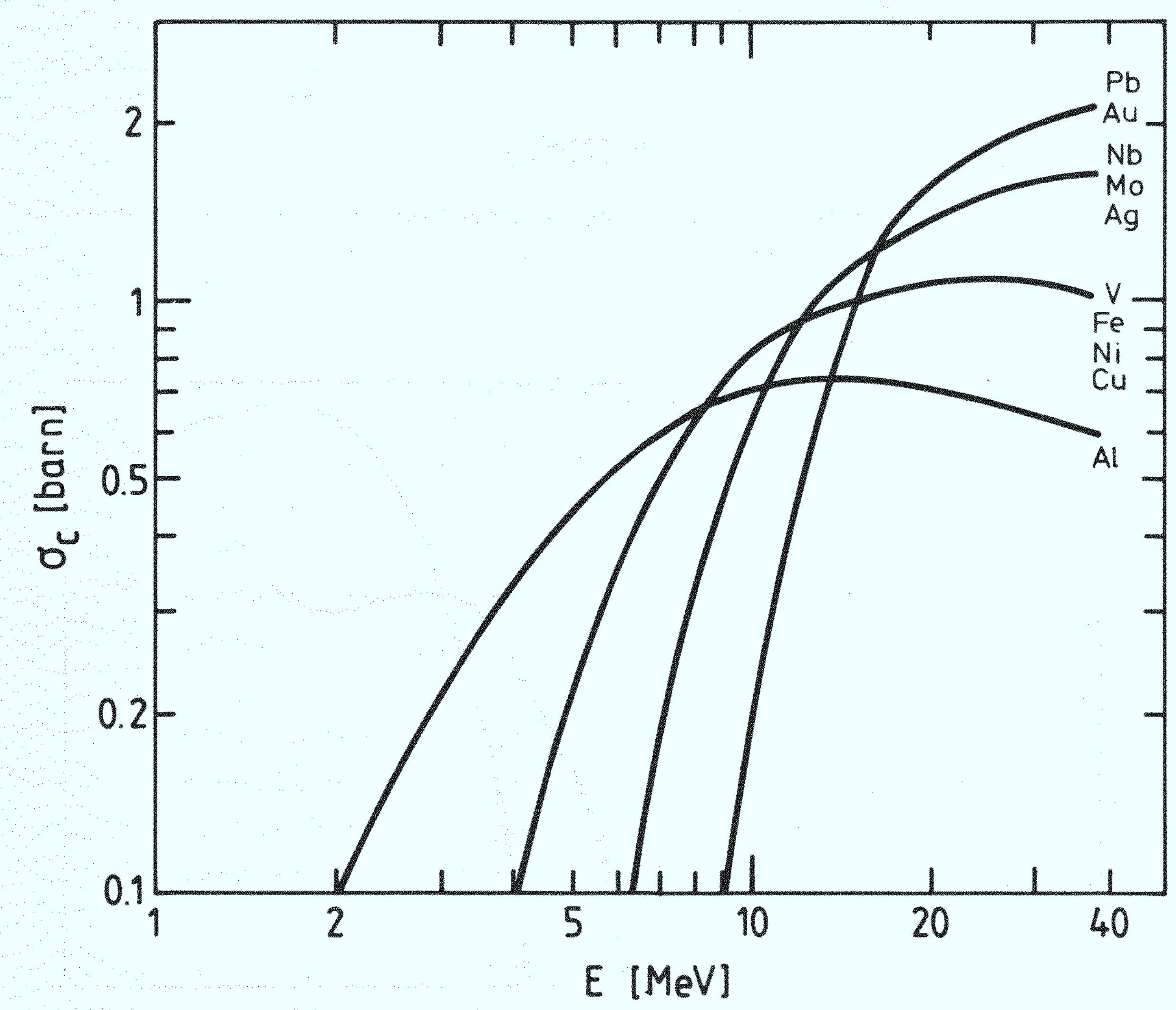

Fig. 2: Averaged cross sections for compound nuclear reactions of protons as a function of energy.

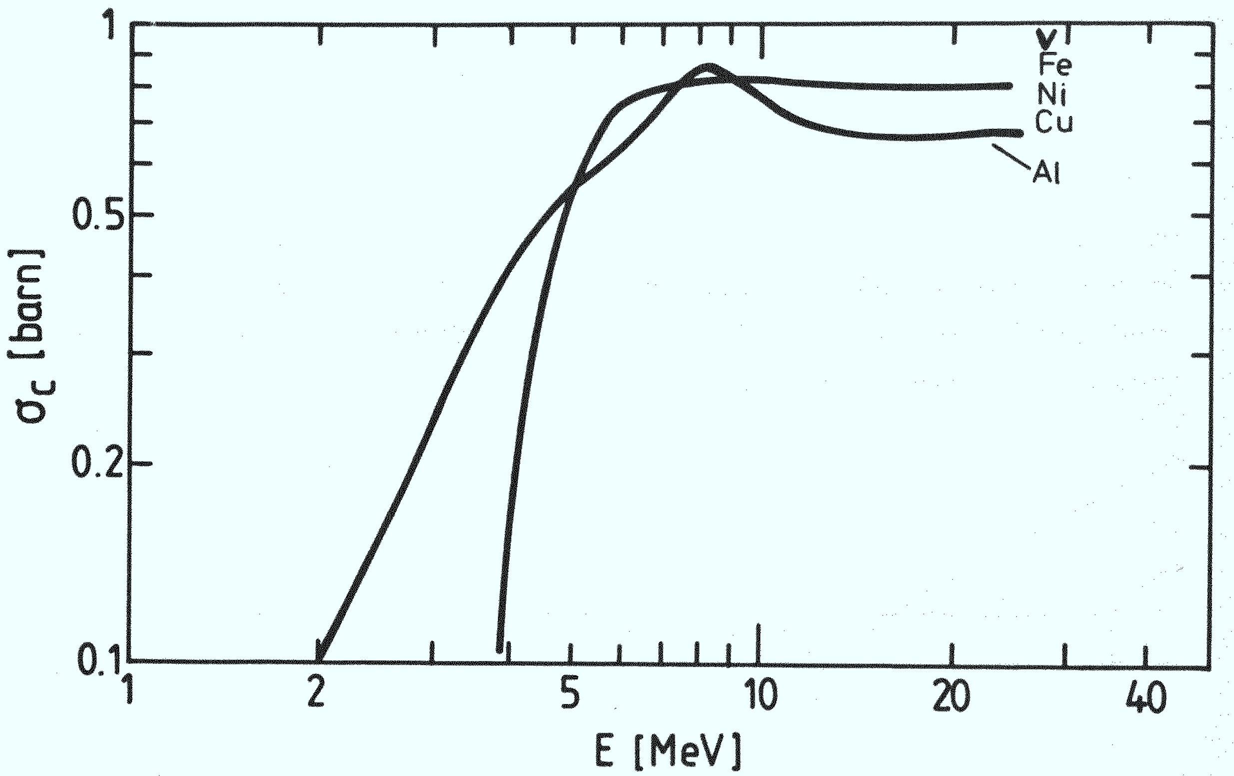

Fig. 3: Averaged cross sections for compound nuclear reactions of deuterons as a function of energy.

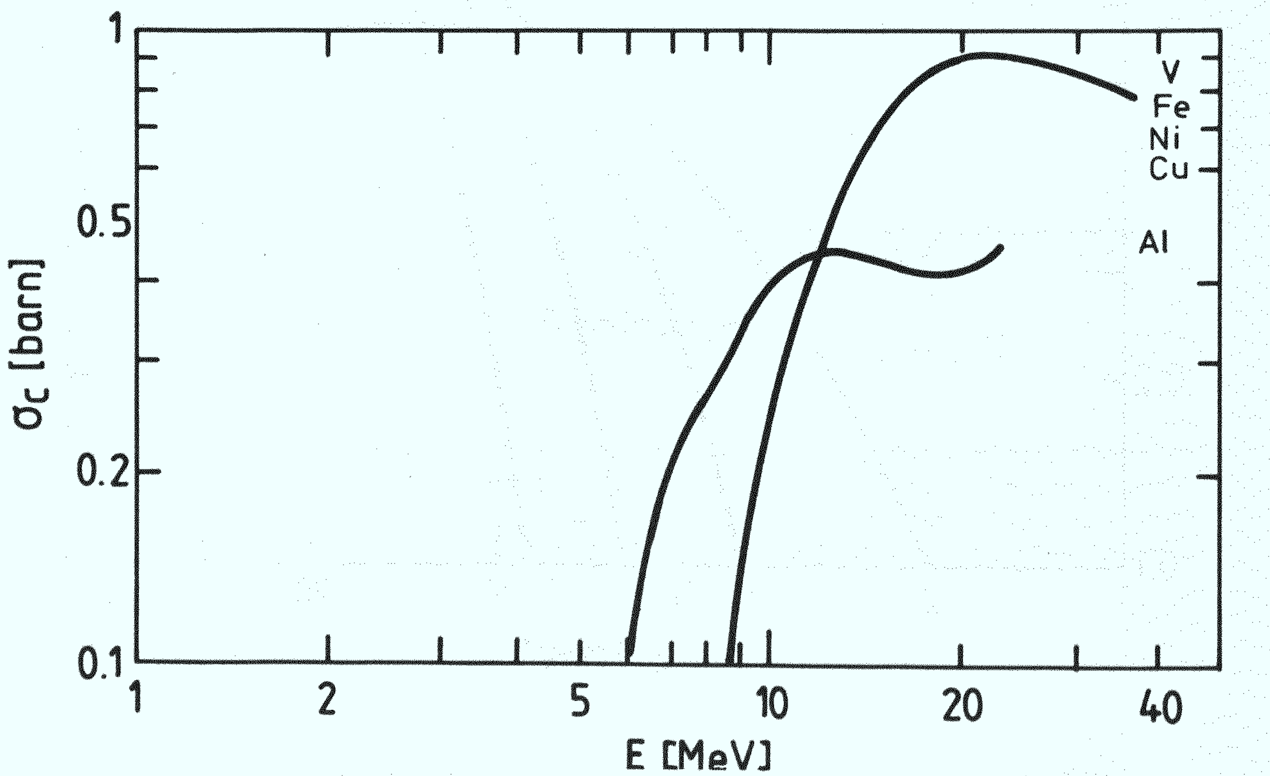

Fig. 4: Averaged cross sections for compound nuclear reactions of α-particles as a function of energy.

III. Displacement function

Besides the differential cross section, the displacement function ν must be known to calculate displacement cross sections from equation (4). For a monoatomic isotropic lattice, the number ν of defects produced by a PKA of energy T is usually estimated from a modified Kinchin-Pease model /21,22/:

$$\nu = \beta \cdot \frac{T/\eta}{2T_d} \tag{18}$$

η accounts for the fact that a certain fraction of the PKA's energy T is lost in electron excitation. An analytical approximation to the theory of Lindhard et al /23/ was given in /24/:

$$\eta = 1+0.1337 \frac{Z^{2/3}}{M^{1/2}} \left(3.4008\tau^{1/6}+0.402\tau^{3/4}+\tau\right) \tag{19}$$

$$\tau = T/(2Z^2 \frac{e^2}{a})$$

β includes the non-hard-sphere character of the interaction of the lattice atoms and according to computer calculation amounts to about 0.8 /24/. T_d is considered as an average atomic displacement energy and can on principle be derived from electron irradiations /2/.

Equation (18) is based on statistical calculations /21/ and computer modelling /24/ which only may be appropriate at high energies T. Furtheron the parameter T_d seems insufficient defined /25,26/ and limitations of the underlying stopping theory /23/ were observed /27/. Therefore in the present work the $\nu(T)$ functions are strictly derived from experimental data, and equation (18) is used only at high energies ($T \gtrsim 5$ keV) where its correctness has been proved /26/. This has been done by a detailled analysis of reactor- and fast neutron results /26/ as well as heavy ion irradiations /28,29/ which both show that equation (18) describes the high energy data within the error bars for a constant empirical parameter $T_d = T_{d,eff}$. These high-energy $T_{d,eff}$-values differ appreciably from average displacement energies at low energies T, derived from electron data /2/. The differences are presumably due to enhanced spontaneous defect recombination in large cascades /30/.

At low energies ($T \lesssim 0.5$ keV) where a statistical model is certainly inapplicable, $\nu(T)$ is directly determined from electron data. This is important in the present case as 25 to 35 % of the defects produced by light ions in the 1-10 MeV range result from single displacement events ($\nu \leq 1$).

In the intermediate energy range (~ 0.5 to 5 keV) an interpolation between the low and the high energy part of the $\nu(T)$-function was derived in a way to fit the available light ion data as closely as possible. Further constraints on $\nu(T)$ were, that the overall function was non-decreasing and as smooth as possible.

In Figs. 5 and 6 it is shown for Cu and Nb that it is actually possible to cover the whole reach of T values up to around 1 MeV by irradiating with electrons, light ions and fast neutrons. The quantity W(T') gives the fraction of defects produced by PKA events of energies below T':

$$W(T') = \frac{1}{\sigma_d} \int_{T_{d,min}}^{T'} \frac{d\sigma}{dT} \cdot \nu(T)\, dT \qquad (20)$$

For non-monoenergetic particles like reactor neutrons, σ_d and the integral in equation (20) must be averaged over the energy spectrum of the particles.

The parameters ρ_F, $T_{d,min}$ and $T_{d,eff}$ used in the present calculations are listed in Table I. The values for ρ_F were taken from diffuse X-ray scattering (Al, Ni, Cu, Mo) and from single-crystal resistivity measurements (Fe, Pt) /31/. For materials where such experimental data are missing, ρ_F was derived from a semi-empirical formula /32/ which describes all presently available ρ_F da-

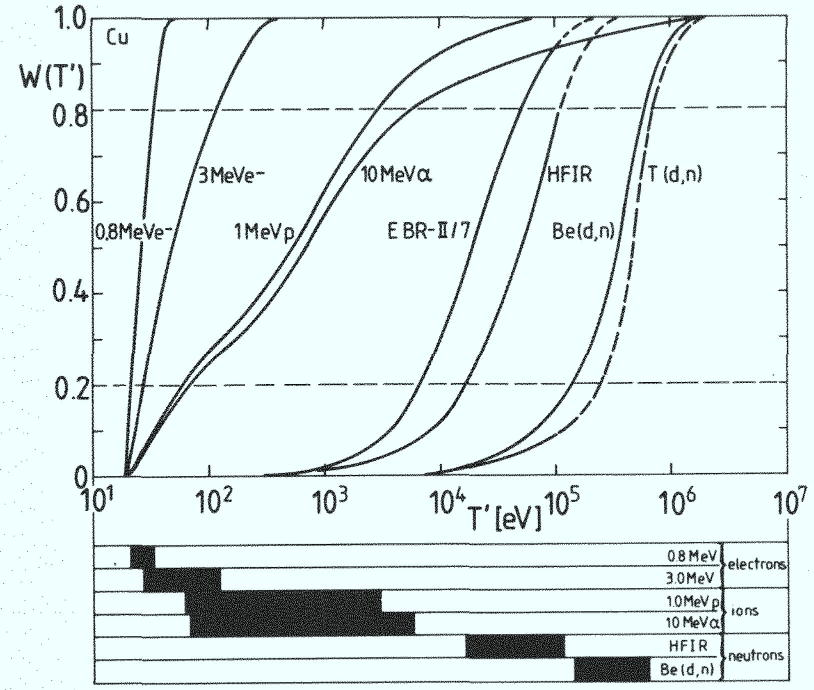

Fig. 5:
Fraction of defects produced by PKA-events of energies below T' for Cu irradiated with different particles. The electron and light ion results are from the present work, the Be(d,n) results from Ref. /3/. The EBR II-7, HFIR and the initial part of the 14 MeV neutron results are from Ref. /33/. These latter results are completed in accordance with calculations for Ni in Ref. /3/ (dashed). The lower part of the figure shows for some of the above spectra the range of energies where 60 % of the defects are produced.

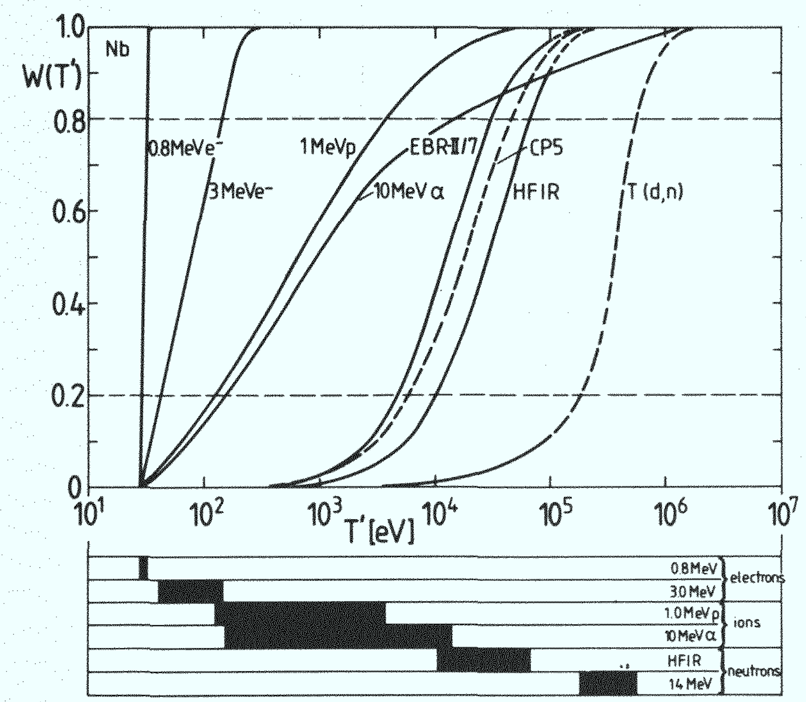

Fig. 6:
Fraction of defects produced by PKA events of energies below T' for Nb. The results for CPS neutrons are from Ref. /3/, other references as in Fig. 5.

ta very well. For some materials (Ag, Au) these semi-empirical ρ_F-values were slightly modified to correspond to values commonly used in the literature.

The values of the minimum displacement energy $T_{d,min}$ are taken from references cited in /34/ and the $T_{d,eff}$ values from neutron data /3,6,7/ collected in table II:

$$T_{d,eff} = \frac{0.8 \quad \rho_F \quad \langle\sigma T\rangle}{2 \cdot \Delta\rho/\Delta\phi} \tag{21}$$

according to equation (18).

As no neutron data are available for Au, $T_{d,eff}$ was derived from self-ion data /29/ which in the case of Ag give reasonable agreement with the results from neutron data.

Table I: Parameters for calculating $\nu(T)$.

	ρ_F [$\mu\Omega m$]	$T_{d,min}$ [eV]	$T_{d,eff}$ [eV]	$\frac{T_{d,eff}}{T_{d,min}}$
Al	4	16	75	4.7
V	22	25	121	4.8
Fe	30	17	183	10.8
SS	25	18+	120	6.7
Ni	7°	23	142	6.2
Cu	2	19	100	5.3
Nb	16	28	150	5.4
Mo	14	34	159	4.7
Pd	9	34	138	4.1
Ag	2.1	24	113	4.7
Ta	17	32	148	4.6
W	18	40	107	2.7
Pt	10	34	138	4.1
Au	2.5	34	110*	3.2

o Ref. /67/

+Ref. /35/

*from self-ion data /29/.

Table II: Damage Rates from Moderated and Unmoderated Fission Spectra (damage rates $\frac{\Delta\rho}{\Delta\phi}$ in 10^{-31} Ωm^3, damage energy cross section $\langle\sigma T\rangle$ in barn-kev, $T_{d,eff}$ in eV).

	ANL-CP5-VI53[a]			LLL-LPTR-FNIF10[b]			ORNL-BSR-LTIF[c]			
	$\frac{\Delta\rho}{\Delta\phi}$	$\langle\sigma T\rangle$	$T_{d,eff}$	$\frac{\Delta\rho}{\Delta\phi}$	$\langle\sigma T\rangle$	$T_{d,eff}$	$\frac{\Delta\rho}{\Delta\phi}$	$\langle\sigma T\rangle$	$T_{d,eff}$	$\langle T_{d,eff}\rangle$
Al	1.49	76.2	82.	-	-	-	2.19	98.9	72.	77±7
V	-	-	-	6.56	79.2	106.	7.17	99.	121.	114±10
Fe	3.33	50.7	183.	-	-	-	-	-	-	183
Ni	1.14	59.0	145.	-	-	-	1.71	85.4	140.	142±3
Cu	0.424	56.3	106.	-	-	-	0.723	82.1	91.	98±11
Nb	2.19	55.7	163.	3.47	60.3	111.	3.43	81.	151.	142±27
Mo	1.86	61.2	184.	3.00	69.5	130.	3.38	85.7	142.	152±28
Pd	-	-	-	-	-	-	1.90	73.	138.	138
Ag	0.295	47.3	135.	-	-	-	0.666	72.	91.	113+22
Ta	-	-	-	-	-	-	2.52	54.7	148.	148
W	-	-	-	-	-	-	4.2	52.2	89.	89
Pt	0.818	29.6[e]	145.	-	-	-	1.59	45.8[e]	115.	130±21

Damage Rates from Fast Neutrons (units as above)

	Be(40 MeV-d,n)[d]			Be(30 MeV- d,n)[b]			T(d,n)-RTNS[b]			
	$\frac{\Delta\rho}{\Delta\phi}$	$\langle\sigma T\rangle$	$T_{d,eff}$	$\frac{\Delta\rho}{\Delta\phi}$	$\langle\sigma T\rangle$	$T_{d,eff}$	$\frac{\Delta\rho}{\Delta\phi}$	$\langle\sigma T\rangle$	$T_{d,eff}$	$\langle T_{d,eff}\rangle$
Al	-	-	-	-	-	-	4.2	179.	70.	70.
V	-	-	-	14.0[+]	200.	125.	18.0[+]	267.	134.	130±6
Cu	2.11	265.	100.	-	-	-	2.5	288.	100.	109±1
Nb	10.1	243.	154.	7.4	197.	173.	11.4	263.	149.	159±13
Mo	-	-	-	6.1[+]	192.	179.	9.5[+]	263.	158.	169±15
W	-	-	-	-	-	-	11.55	201.	125.	125.
Pt	4.72	182.[e]	154.	-	-	-	-	-	-	154.

[+] corrected for initial transients, consonant with Ref. /6/

a) data from Ref. /36/, Nb-data from Ref. /37/, calculations Ref. /3/

b) Ref. /7/

c) data and calculations Refs. /6/

d) data from Ref. /38/, calculations from Ref. /7/

e) $\langle\sigma T\rangle$ calculation from Ref. /7/

IV. Results

Displacement functions $\nu(T)$ have been derived from experimental damage rate data for:

Al, V, Fe, Cu, Nb, Mo, Ag, Pt and Au,

and are given in Figs. 7 to 9. The first bar on the different curves indicates the extent of transferred energies in the electron irradiation, while the second and third bar indicate the reach of average transferred energies in reactor and fast neutron irradiations, respectively. These latter range can be roughly approximated for Al, V, Cu, Nb, Mo and Pt by /26/:

$$\frac{0.83}{Z} \lesssim T[\mathrm{MeV}] \lesssim \frac{13.5}{Z} \qquad (22)$$

The damage rates calculated from these $\nu(T)$-functions are compared to experimental electron and light ion data in appendix A (Figs. A 1-A9).

Fig. 10 shows $\nu(T)$ for Fe, Ni and stainless steel as a function of the damage energy $T_D = T/\eta$. In the case of Ni reasonable electron- and neutron data exist, giving the lower and upper part of the Ni curve. As light ion data for Ni are missing, the intermediate range of $\nu(T)$ was interpolated according to some average curve of Figs. 7 and 8. For stainless steel only damage rate measurements for neutrons are reported /6/. From the semi-empirical equation /32/ ρ_F = 25 μΩm is deduced for stainless steel /26/, giving a $T_{d,eff}/T_{d,min}$ value for stainless steel almost identical to the value of nickel. That means the upper parts of the $\nu(T)$ curves of these two metals fall close together (Fig. 10). This and the similarity of all other $\nu(T_D/T_{d,min})$ curves is encouraging to use the Ni-curve for stainless steel. On the other hand Fig. 10 also shows that the $\nu(T)$ curve recommended in the NRT-proposal /24/ is in the high energy part by a factor of about three too high.

Numerical data of the normalized damage rates are given in tables III a, b and c for protons, deuterons and α-particles, respectively. Values in paranthesis are extrapolations when

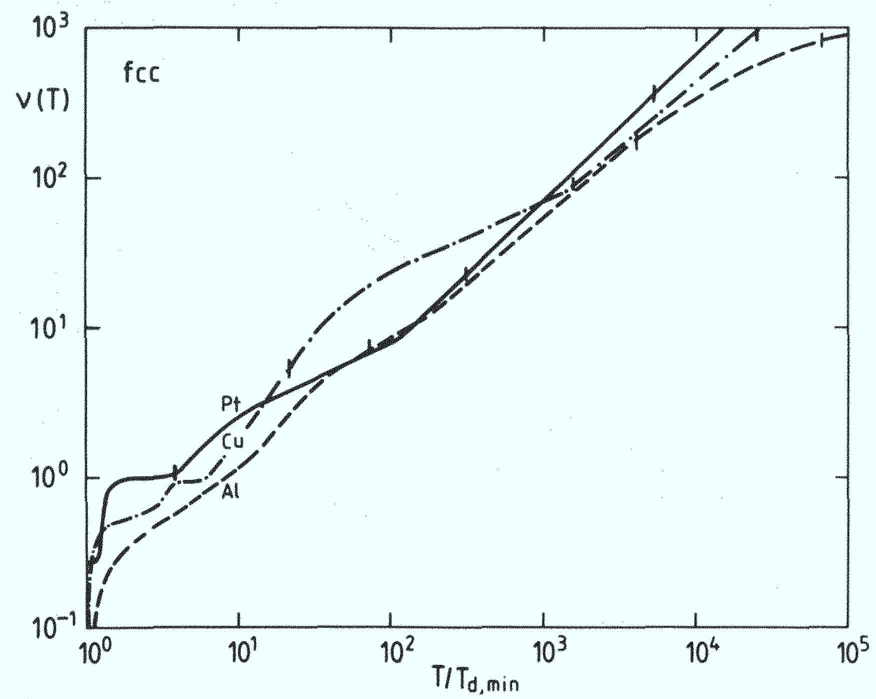

Fig. 7: Displacement functions ν(T) for Al, Cu and Pt as a function of transferred energy, in units of the minimum displacement energy. The first bar on each curve, indicates the extent of electron irradiations, the second and third bar indicates the reach of the average transferred energies in the neutron irradiations.

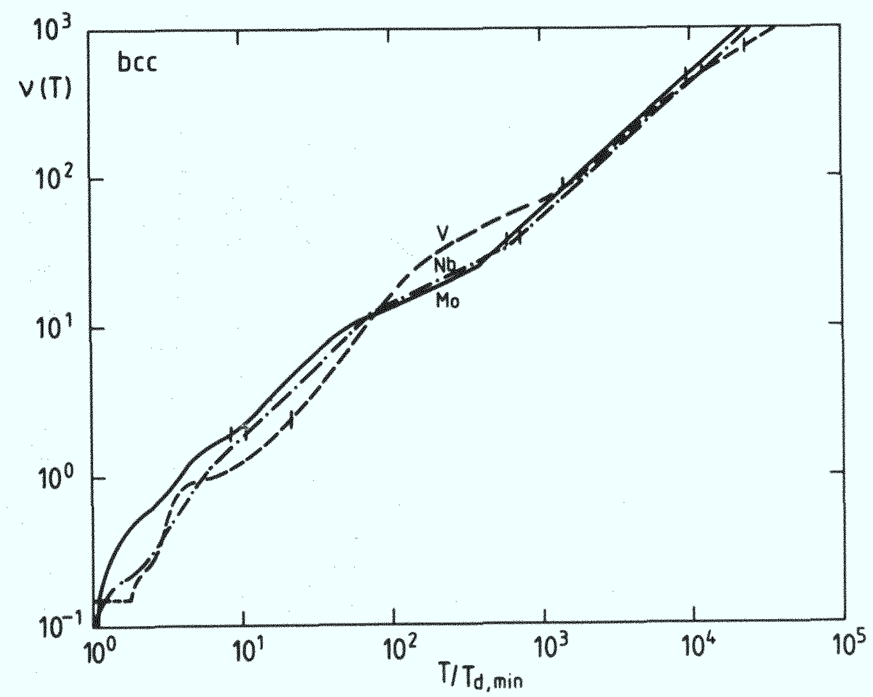

Fig. 8: Displacement functions ν(T) for V, Nb and Mo as a function of transferred energy in units of the minimum displacement energy. The bars on the curves are explained under Fig. 7.

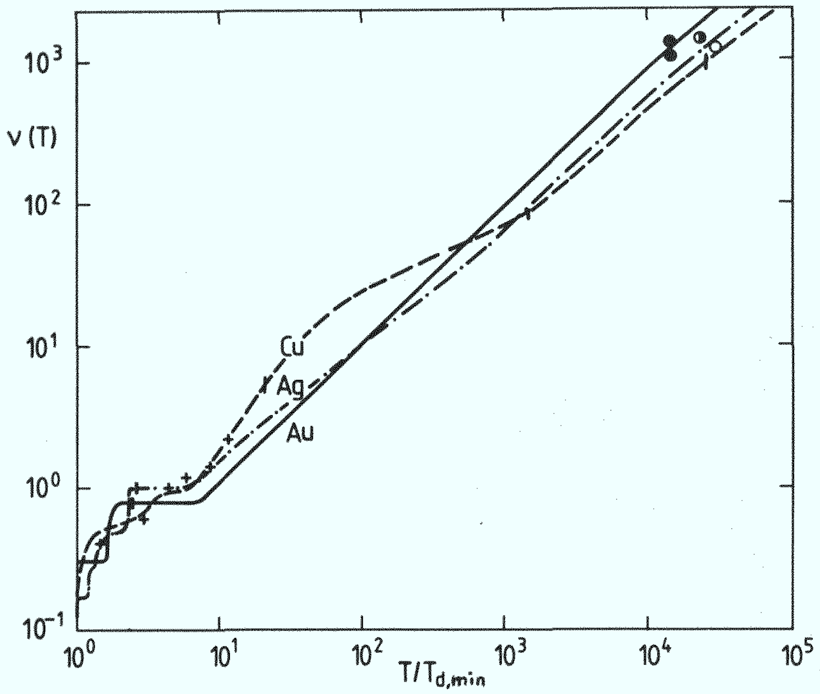

Fig. 9: Displacement functions $\nu(T)$ for Cu, Ag and Au as a function of transferred energy in units of the minimum displacement energy. The bars on the curves are explained under Fig. 7. The circles give $\nu(T)$ data from self ion irradiations /29/ for Cu (O), Ag (◑) and Au (●). For Au $\nu(T)$ was fitted to those data, as no neutron data were available. Included are results from computer calculations (+) for Cu /39/.

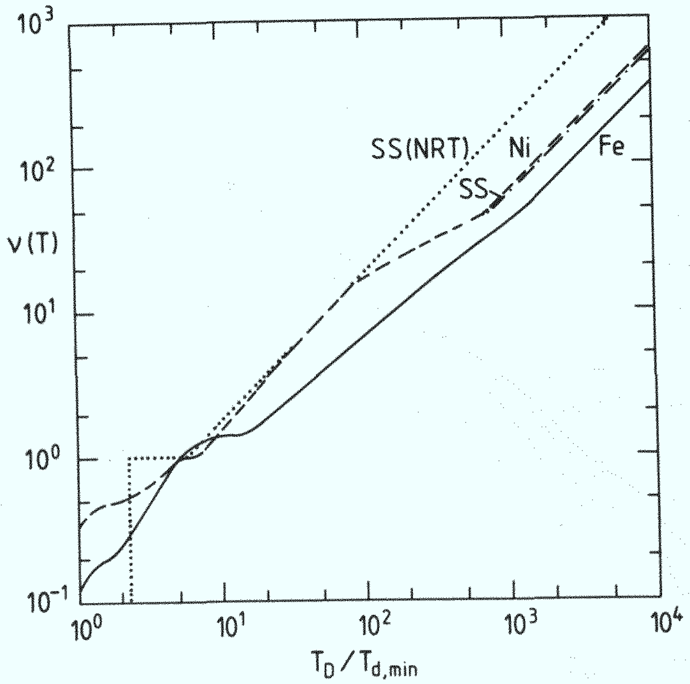

Fig. 10: Displacement functions $\nu(T)$ for Fe (-), Ni (--) and stainless steel (-·-) as a function of damage energy T_D in units of the minimum displacement energy. The dotted line gives $\nu(T)$ of the modified Kinchin-Pease model /24/ with $T_{d,min}$ = 18 eV and $T_{d,eff}$ = 40 eV (for stainless steel).

Table IIIa: Normalized damage rates $\frac{\Delta\rho}{\Delta\phi}\frac{E}{mz^2}$ [10^{-23} $\Omega\,cm^3$ MeV] for protons ($mz^2 = 1$)

E[MeV]	Al	V	Fe	SS	Ni	Cu	Nb	Mo	Pd	Ag	Ta	W	Pt	Au
0.0005	0.067	0.054	0.166	0.297	0.040	0.018	-	-	-	-	-	-	-	-
0.001	0.130	0.210	0.550	0.826	0.166	0.065	0.060	0.015	0.044	0.015	-	-	-	-
0.002	0.216	0.638	1.38	1.63	0.353	0.137	0.251	0.246	0.479	0.092	0.065	0.001	0.042	0.011
0.005	0.348	1.27	2.68	2.98	0.670	0.279	0.865	0.909	1.17	0.235	0.601	0.544	0.849	0.141
0.01	0.456	1.82	3.65	4.40	0.982	0.450	1.59	1.60	1.84	0.367	1.36	1.48	1.65	0.272
0.02	0.543	2.46	4.61	5.95	1.34	0.658	2.45	2.39	2.51	0.513	2.48	2.70	2.72	0.405
0.05	0.638	3.50	5.76	8.02	1.82	0.915	3.68	3.50	3.28	0.704	4.27	4.57	4.11	0.611
0.1	0.702	4.26	6.50	9.36	2.11	1.06	4.53	4.20	3.75	0.836	5.57	6.07	5.00	0.777
0.2	0.759	4.83	7.14	10.4	2.33	1.17	5.16	4.72	4.16	0.951	7.06	7.29	5.73	0.941
0.5	0.822	5.33	7.81	11.3	2.54	1.26	5.74	5.22	4.64	1.08	8.30	8.64	6.58	1.15
1.0	0.862	5.62	8.22	11.8	2.67	1.32	6.11	5.54	4.96	1.16	9.01	9.58	7.15	1.29
2.0	0.921	5.87	8.56	12.3	2.78	1.37	6.44	5.83	5.23	1.23	9.67	10.5	7.67	1.42
5.0	1.041	6.19	8.94	12.8	2.91	1.43	(6.82)	6.17	5.55	1.32	10.4	11.5	8.27	1.58
10.0	1.12	(6.8)	(9.42)	(13.3)	3.02	1.47	(7.08)	(6.39)	(5.76)	(1.37)	11.0	(12.3)	(8.68)	(1.70)
20.0	(1.34)	(7.7)	(11.0)	(15.3)	3.20	(1.64)	(7.30)	(6.58)	(5.94)	(1.42)	(11.5)	(13.0)	(9.04)	(1.80)

Table IIIb: Normalized damage rates $\frac{\Delta\rho}{\Delta\phi} \frac{E}{mz^2}$ [10^{-23} Ω cm^3 MeV] for deuterons ($mz^2 = 2$)

E[MeV]	Al	V	Fe	SS	Ni	Cu	Nb	Mo	Pd	Ag	Ta	W	Pt	Au
0.0005	0.076	0.110	0.281	0.426	0.085	0.033	0.028	0.006	0.017	0.007	-	-	-	-
0.001	0.138	0.382	0.801	0.934	0.201	0.077	0.134	0.132	0.253	0.048	0.030	0.001	0.020	0.005
0.002	0.228	0.751	1.55	1.66	0.371	0.148	0.404	0.426	0.579	0.115	0.237	0.179	0.333	0.053
0.005	0.366	1.39	2.68	3.19	0.708	0.325	1.12	1.12	1.23	0.244	0.850	0.933	1.01	0.165
0.01	0.462	2.02	3.63	4.68	1.05	0.521	1.88	1.83	1.83	0.373	1.73	1.89	1.84	0.271
0.02	0.546	2.81	4.59	6.30	1.43	0.727	2.80	2.67	2.44	0.517	2.91	3.14	2.80	0.408
0.05	0.646	3.90	5.74	8.32	1.88	0.946	4.01	3.70	3.16	0.707	4.82	5.11	4.04	0.625
0.1	0.713	4.54	6.50	9.49	2.14	1.07	4.72	4.30	3.65	0.839	6.22	6.43	4.86	0.801
0.2	0.772	5.00	7.15	10.4	2.34	1.15	5.26	4.77	4.10	0.962	7.33	7.59	5.64	0.975
0.5	0.835	5.45	7.84	11.3	2.55	1.26	5.85	5.29	4.63	1.09	8.48	9.03	6.58	1.19
1.0	0.872	5.74	8.27	11.9	2.69	1.33	6.23	5.64	4.98	1.18	9.24	10.0	7.21	1.35
2.0	0.899	5.99	8.63	12.3	2.81	1.38	6.58	5.94	5.28	1.26	9.93	10.9	7.77	1.49
5.0	0.923	6.2	9.01	12.8	2.94	1.43	(6.97)	(6.29)	5.62	1.34	10.7	12.0	8.42	1.65
10.0	1.00	(6.5)	(9.40)	13.1	3.01	1.42	(7.22)	(6.51)	5.83	1.40	(11.3)	(12.8)	(8.84)	(1.72)
20.0	(1.05)	(6.8)	(10.2)	(13.5)	3.1	(1.44)	(7.43)	(6.69)	(6.01)	(1.45)	(11.8)	(13.5)	(9.22)	(1.87)

Table IIIc: Normalized damage rates $\frac{\Delta\rho}{\Delta\phi}\frac{E}{mz^2}$ $[10^{-23}\ \Omega cm^3\ MeV]$ for α-particles (mz^2 = 16)

E[MeV]	Al	V	Fe	SS	Ni	Cu	Nb	Mo	Pd	Ag	Ta	W	Pt	Au
0.0005	0.038	0.091	0.181	0.209	0.044	0.017	0.027	0.027	0.050	0.009	0.005	0.000	0.003	0.001
0.001	0.077	0.222	0.431	0.444	0.098	0.039	0.098	0.103	0.136	0.027	0.050	0.037	0.069	0.011
0.002	0.143	0.443	0.803	0.904	0.197	0.088	0.274	0.278	0.288	0.057	0.158	0.171	0.192	0.032
0.005	0.250	0.971	1.58	2.05	0.455	0.231	0.762	0.728	0.658	0.133	0.556	0.617	0.561	0.081
0.01	0.338	1.63	2.36	3.32	0.747	0.392	1.39	1.30	1.05	0.223	1.17	1.26	1.04	0.147
0.02	0.429	2.45	3.24	4.83	1.08	0.562	2.21	2.01	1.50	0.339	2.13	2.28	1.66	0.250
0.05	0.547	3.48	4.44	6.68	1.50	0.768	3.27	2.92	2.17	0.515	3.80	3.91	2.63	0.442
0.1	0.631	4.10	5.31	7.89	1.77	0.901	3.97	3.54	2.72	0.653	5.03	5.19	3.46	0.617
0.2	0.705	4.60	6.11	8.94	2.01	1.02	4.61	4.11	3.27	0.787	6.14	6.52	4.34	0.806
0.5	0.785	5.18	7.03	10.2	2.31	1.15	5.37	4.81	3.97	0.955	7.54	8.25	5.49	1.06
1.0	0.831	5.55	7.63	11.0	2.50	1.24	5.88	5.27	4.44	1.07	8.52	9.47	6.31	1.24
2.0	0.866	5.85	8.14	11.6	2.66	1.31	6.33	5.68	4.87	1.18	9.42	10.6	7.07	1.41
5.0	(0.898)	6.15	8.66	12.3	2.83	1.39	6.82	6.13	5.34	1.29	10.5	11.9	7.95	1.62
10.0	(0.914)	(6.3)	(8.95)	(12.7)	2.90	(1.43)	(7.12)	6.40	(5.63)	(1.37)	11.1	12.8	8.52	1.75
20.0	(0.925)	(6.4)	(9.5)	(13.0)	2.95	(1.41)	(7.36)	(6.61)	(5.86)	(1.42)	(11.7)	(13.6)	(9.01)	(1.87)

nuclear cross section data were missing. Included in these tables are also the metals Pd, Ta and W for which only limited neutron data (Table II) and scarce electron data exist. For these metals the $\nu(T)$ curves in the intermediate energy range were interpolated according to metals which are similar in their low as well as high energy behaviour. There were Pt in the case of Pd, Nb in the case of Ta and Mo in the case of W. For further metals approximate damage rates can be calculated by using an average displacement function derived from Figs. 7-9.

$$\nu(T) = 0.15 + 1.5 \; \frac{(T/T_{d,min}{}^{-1})^{0.8}}{T_{d,eff}/T_{d,min}} \qquad (23)$$

Table I shows that for most metals a further relation approximately holds:

$$\frac{T_{d,eff}}{T_{d,min}} \approx 5 \pm 1 \qquad (24)$$

The few exceptions (Fe, W, Au) are at moment not well enough examined to be taken too serious.

Mainly in fusion reactors the production of helium by nuclear reactions may become a serious problem for structural integrity. Light ion irradiations offer two possibilities to introduce helium to simulate the processes in first wall materials:

i) At energies above the coulomb barrier (7) protons and deuterons produce helium by transmutation in a similar way as neutrons do. In appendix B cross sections σ_α for α-production by (p,α), $(p,\alpha n)$, (d,α) etc. processes are collected from /10,11,40/ and plotted in Figs. B1-B6 for those metals which seem of potential interest for fusion reactor application. The helium-to-dpa ratio σ_α/σ_d is included in the figures. This ratio is supposed to be an important parameter to describe material behaviour in a fusion environment. It must be emphasized that most of the σ_α-data in /40/ are only interpolated from experimental data and therefore may contain appreciable errors.

ii) Implantation of α-particles is a technique to accumulate helium orders of magnitude faster than under fusion reactor conditions. This simulation technique also couples helium production to displacement damage, at least for implantation depths above about 10 nm. Therefore the present damage rate data were used to calculate the number of defects N_d^α produced during the implantation of helium (α-particles) of energy E:

$$N_d^\alpha(E) = N_t \int_0^{l_o} \sigma_d \, dl \qquad (25)$$

l_o is the total path length of the α-particles in the target material. Data on the energy dependence of l_o were taken from /41/ and /42/.

For noble metals the results are plotted in Fig. 11 and compared for Cu and Ag to experimental results /28/. For Ag the agreement is perfect, while for Cu the calculations are slightly above the data. This is consistent with the damage rate data where the results of Ref. /28/ are also below the calculated curves (Fig. A4), which are mainly aimed to fit the results of Ref. /4/. Numerical results for N_d^α for the other metals are given in Table IV.

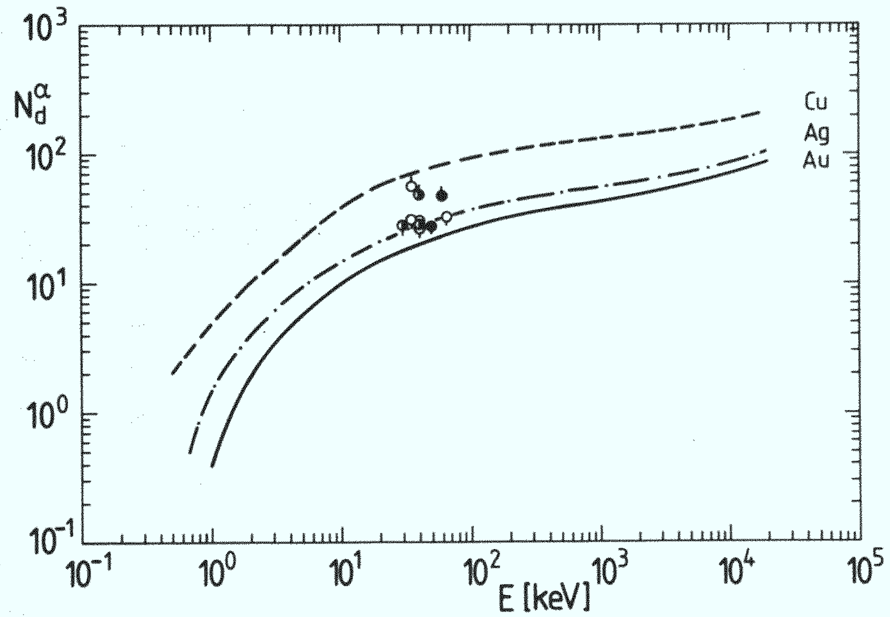

<u>Fig. 11:</u> Number of Frenkel defects produced during implantation of α-particles of energy E in Cu, Ag and Au. The symbols give experimental results of Ref. /28/ for Cu (ȯ, ◐, ●) and Ag (♀, ♀, ♀).

Table IV: Number of Frenkel defects produced during implantation of α-particles

E[MeV]	Al	V	Fe	SS+	Ni	Cu	Nb	Mo	Pd	Ag	Ta	W	Pt	Au
0.0005	2.6	0.5	1.0	1.6	1.2	2.1	0.1	<0.1	0.1	0.1	<0.1	<0.1	<0.1	<0.1
0.001	5.8	1.4	2.5	3.5	2.7	4.9	0.4	0.4	1.6	1.5	0.1	<0.1	0.4	0.4
0.002	10.9	3.0	4.9	6.7	5.4	10.2	1.3	1.4	4.5	3.9	0.7	0.6	2.27	1.9
0.005	21.1	6.6	10.2	14.1	11.7	23.1	3.7	4.3	10.1	9.1	2.6	2.7	6.25	5.8
0.01	29.0	10.7	15.2	22.6	19.1	43.0	7.0	7.6	17.7	14.6	5.7	6.4	13.5	9.8
0.02	36.7	15.5	20.9	32.5	27.6	58.9	11.0	13.1	23.6	21.5	9.2	10.5	19.9	14.9
0.05	44.4	21.7	27.6	45.4	38.7	83.6	16.5	18.7	32.3	31.0	15.7	17.3	30.5	22.8
0.1	49.3	26.1	32.2	54.8	46.8	98.8	20.9	23.3	38.9	37.9	21.1	23.0	38.1	28.4
0.2	54.4	30.0	36.6	62.1	53.2	112.	24.8	27.4	44.5	43.5	26.6	28.0	45.1	33.4
0.5	59.2	34.7	42.2	72.4	62.1	126.	29.6	32.9	52.7	51.6	33.4	35.6	54.1	40.0
1.0	63.9	37.5	45.0	77.7	66.7	135.	32.6	36.2	56.9	56.1	37.5	39.8	58.9	44.3
2.0	67.7	41.2	48.7	84.1	72.4	146.	36.7	40.4	62.4	61.9	43.0	45.2	65.6	49.5
5.0	(77.4)	49.0	56.3	96.1	83.0	165.	45.1	49.1	74.9	73.8	53.5	56.2	78.5	59.5
10.0	(89.0)	(57.9)	65.5	(110.)	(95.5)	(186.)	(55.2)	59.8	(90.2)	(87.6)	65.5	67.6	93.3	70.4
20.0	(110.)	(73.3)	78.9	(132.)	(110.)	(216.)	(72.0)	(76.0)	(115.)	(108.)	(81.3)	(83.9)	(113.)	(88.2)

+ range data from Fe

V. Discussion

From the results in the last chapter it is seen that for all metals, $\nu(T)$ curves can be derived which are in reasonable agreement with experimental data. In those metals where reliable data over a wide energy range exist for electrons, ions and neutrons, $\nu(T)$ is determined within rather narrow limits under the assumptions that it is smooth and non-decreasing. Unfortunately in some of the well investigated metals - like Cu - data scatter appreciably, introducing a possible error to the calculations.

If compared to the modified Kinchin-Pease (NRT) - model the present $\nu(T)$ curves show that a constant T_d value over the whole energy range is inappropriate, but that the average displacement energy initially decreases with recoil energy T, before it increases again at very high energies. A qualitative explanation of the initial decrease is possible in terms of an antithetical behaviour of single and multiple displacement as suggested in Ref. /25/. The basic idea is that those lattice directions which are relatively "hard" against single atomic displacement - at low energies - are relatively "soft" for multiple displacement - at high energies. That means a relatively high contribution of multiple displacements along those "hard" directions raises the average displacement rate at $\nu > 1$ above the value expected from the low energy T_d values. The final increase of T_d may be due to enhanced recombination in large cascades /30/.

The $\nu(T)$ curves in the present work were derived for defect production at liquid helium temperature. At elevated temperatures defects become mobile and may recombine or agglomerate. In this case, for most material properties, no longer the total amount of defect production may be significant but the fraction of defects which escapes recombination with their own cascade. Only those escaping defects are able to migrate over longer distances and interact with impurities, dislocations or void nuclei and thus promote segregation, irradiation creep or swelling.

Only one attempt has been made so far to determine the temperature dependence of the defect production process /43/. The results indicate that the average displacement energy (T_d) of Ni from helium- to room temperature is reduced by less than 10 eV.

Experimental results to estimate the fraction of escaping defects are scarce and limited essentially to Cu and Al:

1) At irradiation temperatures just above annealing stage I where interstitials become mobile, only 40 % of the interstitials produced in copper by electron irradiation survive recombination with their own vacancy /44/.

2) The survival rate increases with temperature /43,45,46/. Extrapolation of these data suggests that for electron irradiations above room temperature the production rate of freely migrating defects approaches the total defect production rate at helium temperature.

3) Under neutron irradiation of Cu at temperatures above stage I, only 15 % of the interstitials escape recombination or agglomeration with defects of their own cascade /47/. The ratio of the surviving fractions above stage I for neutrons (15 %) versus electrons (40 %) of 0.37 is very close to the corresponding ratio (efficiency) at temperatures below stage I of about 0.35 /26,28/. This similarity was predicted from a simple cascade annealing model /48/.

Therefore, as long as no experimental results in the technically interesting temperature range above 300 $^{\circ}$C are available, it seems reasonable to use the $\nu(T)$ functions derived at helium temperature. In an intermediate temperature range this may lead to an overestimation of the absolute production rates of freely migrating defects, but the relative rates for different irradiation particles are probably still quite reasonable.

VI. Application to simulation experiments

It was the aim of the present work to provide a basis for calculating defect production rates under light ion irradiations. Applications to simulation experiments are straightforward:

a) A consistent data base of 'best-possible' displacement cross sections avoids deviating dpa-calculations by different experimentalists and therefore allows better comparison of experimental results on property changes under irradiation.

b) Comparison of displacement cross sections of different particles facilitates the choice of the most appropriate particle or energy for a certain experiment in terms of displacement rate, helium production rate or He/dpa ratio.

c) The displacement rates given in the present work are derived consistently with displacement rates for fast neutrons /3,7/. This enables a direct comparison of irradiation induced property changes by light ions and fast neutrons on a per-dpa basis.

REFERENCES

/1/ H. Ullmaier, Trans. Inst. Met. 34, 324 (1981).

/2/ P. Jung, Phys. Rev. B23, 664 (1981).

/3/ M.A. Kirk, L.R. Greenwood, J. Nucl. Mater. 80, 159 (1979).

/4/ B.R. Nielsen, Thesis, University of Aarhus (1979); and B.R. Nielsen, H.H. Andersen, J.F. Bak, H. Knudsen, to be published.

/5/ O.S. Oen, Report ORNL-3813 (1965).

/6/ R.R. Coltman, Jr., C.E. Klabunde, J.M. Williams, J. Nucl. Mater. 99, 284 (1981).
and C.E. Klabunde, R.R. Coltman, Jr., J. Nucl. Mater. 108 &109, 183 (1982).

/7/ M.W. Guinan, C.E. Violet, Symposium,on Neutron Cross Sections from 10 - 40 MeV, Brookhaven, 1977, BNL-NCS-50681, p. 361;
and M.W. Guinan, J.H. Kinney, J. Nucl. Mater. 108&109, 95 (1982).

/8/ J. Lindhard, V. Nielsen, M. Scharff, K. Dan. Vidensk. Selsk. Mat. Fys. Medd. 36, No. 10 (1968).

/9/ K.B. Winterbon, P. Sigmund, J.B. Sanders, K. Dan. Vidensk. Selsk. Mat. Fys. Medd. 37, No. 14 (1972).

/10/ D.B. Smith (Ed.), Charged Particle Cross Sections Ne to Cr, Los Alamos Sci. Lab., LA-2424 (1961).

/11/ F.K. McGowan, W.T. Milner, H.J. Kim (Eds.), Nuclear Cross Sections for Charged-Particle Induced Reactions, Oak Ridge Nat. Lab., ORNL-CPX 1,2 (1964).

/12/ V.F. Weisskopf, Phys. Rev. 52, 295 (1937).

/13/ P.C. Gugelot, Phys. Rev. 93, 425 (1954).

/14/ D.G. Doran, Nucl. Science Eng. 49, 130 (1972).

/15/ S.M. Grimes, J.D. Anderson, B.A. Pohl, J.W. McClure, L. Wong, Phys. Rev. 24, 607 (1971).

/16/ A.M. Omar, J.E. Robinson, D.A. Thompson, J. Nucl. Mater. 64, 121 (1977).

/17/ F.G. Perey, Phys. Rev. 131, 745 (1963).

/18/ R.D. Albert, L.F. Hansen, Phys. Rev. 123, 1749 (1961).

/19/ R.E. Pollock, G. Schrank, Phys. Rev. 140, B575 (1965).

/20/ J.F. Janni, Report AD 643 837 (1966).

/21/ G.H. Kinchin, R.S. Pease, Rep. Progr. Phys. 18, 1 (1955).

/22/ R. Sigmund, Appl. Phys. Lett. 14, 114 (1969) and Rev. Romm. Phys. 17, 1079 (1976).

/23/ J. Lindhard, V. Nielsen, M. Scharff, P.V. Thomsen, K. Dan. Vidensk. Selsk. Mat. Fys. Medd. 33, No. 10 (1963).

/24/ M.J. Norgett, M.R. Robinson, I.M. Torrens, Nucl. Eng. Des. 33, 50 (1975).

/25/ P. Lucasson, A. Lucasson, Rad. Effects 39, 195 (1978).

/26/ P. Jung, B.R. Nielsen, H.H. Andersen, J.F. Bak, H. Knudsen, R.R. Coltman, J.W. Williams, M.W. Guinan, C.E. Violet, in 'Effects of Radiation on Materials' (11^{th} Conf., ASTM STP 782, H.R. Brager, J.S. Perrin, Eds.) ASTM 1982, p. 963.

/27/ M.T. Robinson in Radiation Damage in Metals (N.L. Peterson, S.O. Harkness, Eds.) ASM, Metals Park, Ohio 1976, p. 1.

/28/ R.S. Averback, R. Benedek, K.L. Merkle, Phys. Rev. B 18, 4156 (1978), J. Nucl. Mater. 69&70, 786 (1978), Appl. Phys. Lett. 30, 455 (1977).

/29/ W. Kesternich, K.L. Merkle in Proceedings of the Conf. on Applications of Ion Beams to Metals (S.P. Picraux, E.P. Eer Nisse, F.L. Vook, Eds.) Albuquerque 1975, p. 495.

/30/ R.S. Averback, R. Benedek, K.L. Merkle, J. Nucl. Mater. 75, 162 (1978).

/31/ W. Schilling, J. Nucl. Mater. 69&70, 465 (1978).

/32/ P. Jung, Rad. Effects 51, 249 (1980)

/33/ D.M. Parkin, A.N. Goland, Rad. Effects 28, 31 (1976).

/34/ P. Jung, Rad. Effects 35, 155 (1978).

/35/ M.J. Makin , S.N. Buckley, G.P. Walters, J. Nucl. Mater. 68, 161 (1977).

/36/ J.A. Horak, T.H. Blewitt, Phys. Stat. Sol. A9, 721 (1972).

/37/ B.S. Brown, T.H. Blewitt, T.L. Scott, A.C. Klank, J. Nucl. Mater. 52, 215 (1974).

/38/ J.B. Roberto, C.E. Klabunde, J.M. Williams, R.R. Coltman, Jr., Appl. Phys. Lett. 30, 509 (1977).

/39/ J.O. Schiffgens, R.D. Bourquin, J. Nucl. Mater. 69&70, 790 (1978).

/40/ Landolt-Börnstein, Neue Serie Bd. 5b (1973) and 5c (1974).

/41/ J.F. Ziegler "Helium stopping powers and ranges in all elemental matter", Vol. 4, Pergamon Press, 1977.

/42/ L.C. Northcliff, R.F. Schilling, Nuclear Data Tables A7, 233 (1970).

/43/ J. Laakmann, Thesis, RWTH Aachen, (1981).

/44/ D.E. Becker, F. Dworschak, H. Wollenberger, Rad. Effects 17, 25 (1973).

/45/ R. Lennartz, F. Dworschak, H. Wollenberger, J. Phys. F 7, 2011 (1977).

/46/ R.R. Coltman, C.E. Klabunde, J.K. Redman, J. Nucl. Mater. 69&70, 720 (1978).

/47/ U. Theis, H. Wollenberger, J. Nucl. Mater. 88, 121 (1980).

/48/ T.C. Reiley, P. Jung in Radiation Effects in Breeder Reactor Structural Materials (M.L. Bleiberg, J.W. Bennett, Eds.), Conf. Scottsdale 1977, p. 295.

/49/ H.H. Neely, W. Bauer, Phys. Rev. 149, 535 (1966).

/50/ G.W. Iseler, H.I. Dawson, A.S. Mehner, J.W. Kauffman, Phys. Rev. 146, 468 (1968).

/51/ J. Wurm, F. Dworschak, H. Schuster, H. Wollenberger, Rad. Effects 5, 117 (1970).

/52/ K. Herschbach, J.J. Jackson, Phys. Rev. 153, 689 (1967).

/53/ K.L. Merkle, L.R. Singer, Appl. Phys. Lett. 11, 35 (1967).

/54/ P. Jung, G. Lucki, Rad. Effects 26, 99 (1975).

/55/ R.L. Chaplin, K. Sonnenberg, R.R. Coltman, Rad. Effects

27, 119 (1975).

/56/ P.G. Lucasson, R.M. Walker, Phys. Rev. 127, 485 (1962).

/57/ A.M. Omar, J.E. Robinson, D.A. Thompson, J. Nucl. Mater. 84, 173 (1979).

/58/ J. Wurm, Report KFA Jülich, JÜL-581-FN (1969).

/59/ H. Sakairi, E. Yagi, A. Koyama, T. Karasawa, R.R. Hasiguti, J. Phys. Soc. Japan 43, 999 (1977).

/60/ G.D. Magnusson, W. Palmer, J.S. Koehler, Phys. Rev. 109, 1990 (1958).

/61/ H.G. Cooper, J.S. Koehler, J.W. Marx, Phys. Rev. 97, 599 (1955).

/62/ P. Jung, R.L. Chaplin, H.J. Fenzl, K. Reichelt, P. Wombacher, Phys. Rev. B 8, 533 (1973).

/63/ W. Bauer, W.F. Goeppinger, Phys. Rev. 154, 584 (1967).

/64/ E.A. Burke, C.M. Jimenez, L.F. Lowe, Phys. Rev. 141, 629 (1966).

/65/ W. Bauer, A. Sosin, Phys. Rev. 135, A521 (1964).

/66/ K.L. Merkle in Proc. Int. Conf. on Solid State Physics Res. with Accelerators (A.N. Goland, Ed.) New York (1968), 359.

/67/ O. Bender, P. Ehrhart, to be published in J. Phys. F (1983).

A P P E N D I X A

Comparison of calculated damage rates to experimental data under electron and light ion irradiation.

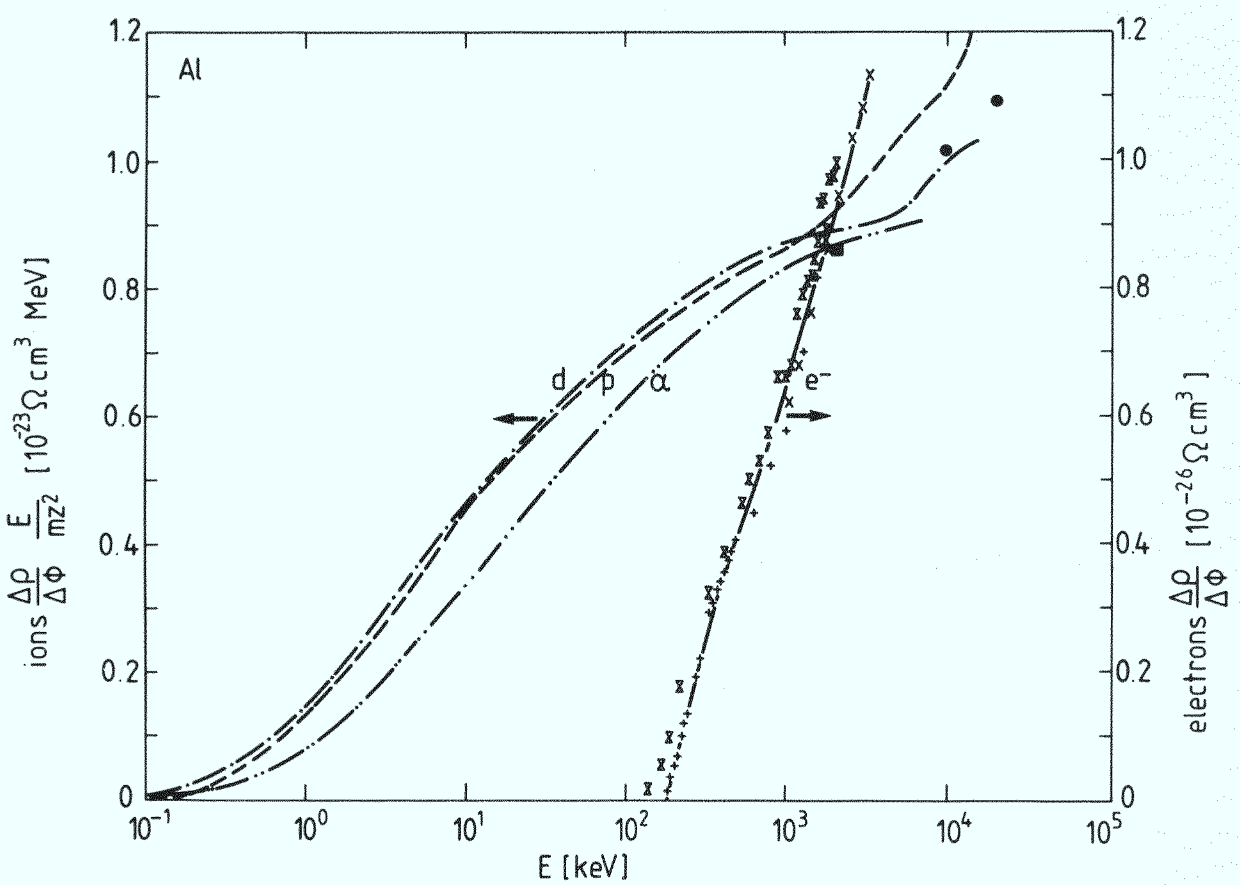

Fig. A1: Damage rates of electrons (+ Ref /49/, x Ref /50/, ⧗ Ref /51/) and normalized damage rates for deuterons (● Ref /52/) and α-particles (■ Ref /53/) in Al as a function of energy. The curves are calculated for electrons (-), protons (--), deuterons (-·-) and α-particles (-··).

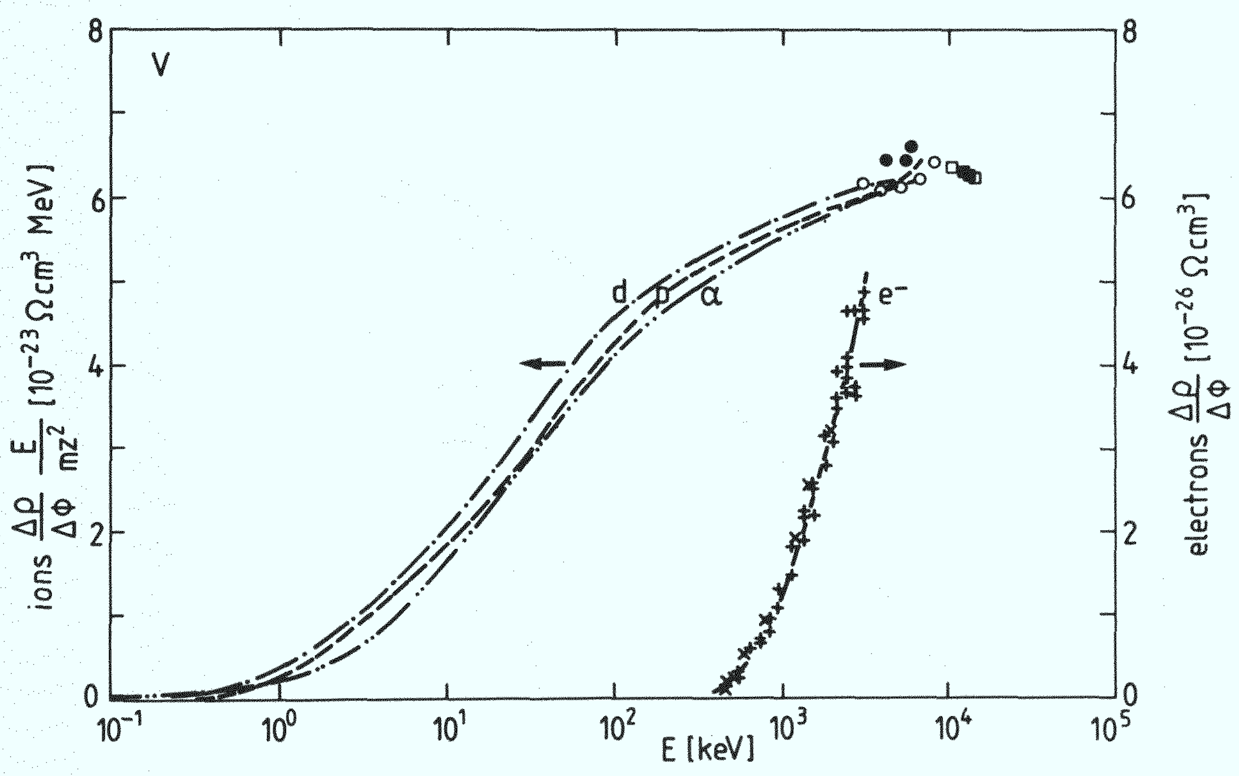

Fig. A2: Damage rates for electrons (+ Ref /54/, x Ref /55/), and normalized damage rates for protons (o), deuterons (●), He^3 (□) and α-particles (■) from Ref /4/ in V as a function energy. The curves are calculated for electrons (——), protons (--), deuterons (-·-) and α-particles (—···-).

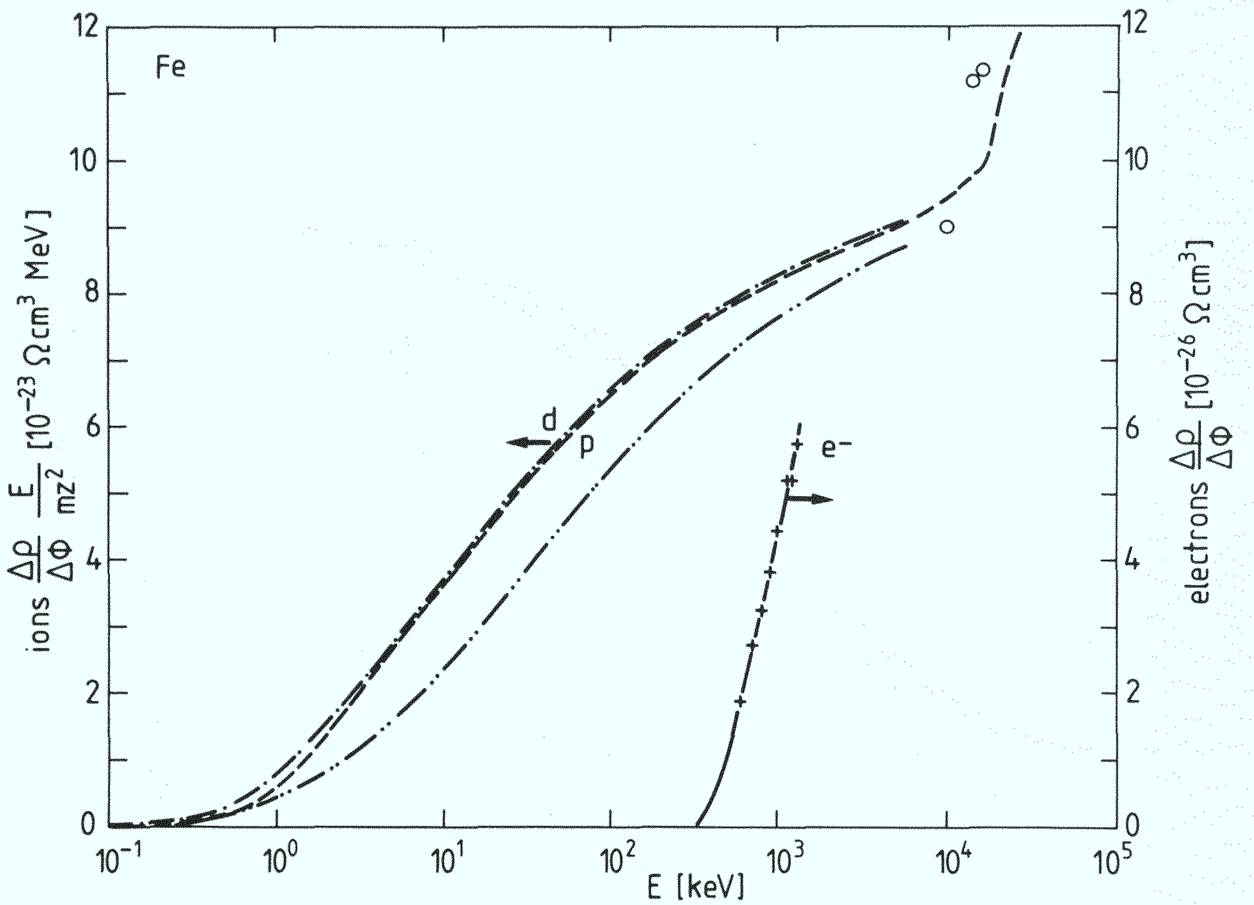

Fig. A3: Damage rates for electron (+ Ref /56/) and normalized damage rates for protons (ǫ Ref /57/) in Fe as a function of energy. The curves are calculated for electrons (——), protons (--), deuterons (-·-) and α-particles (——··-).

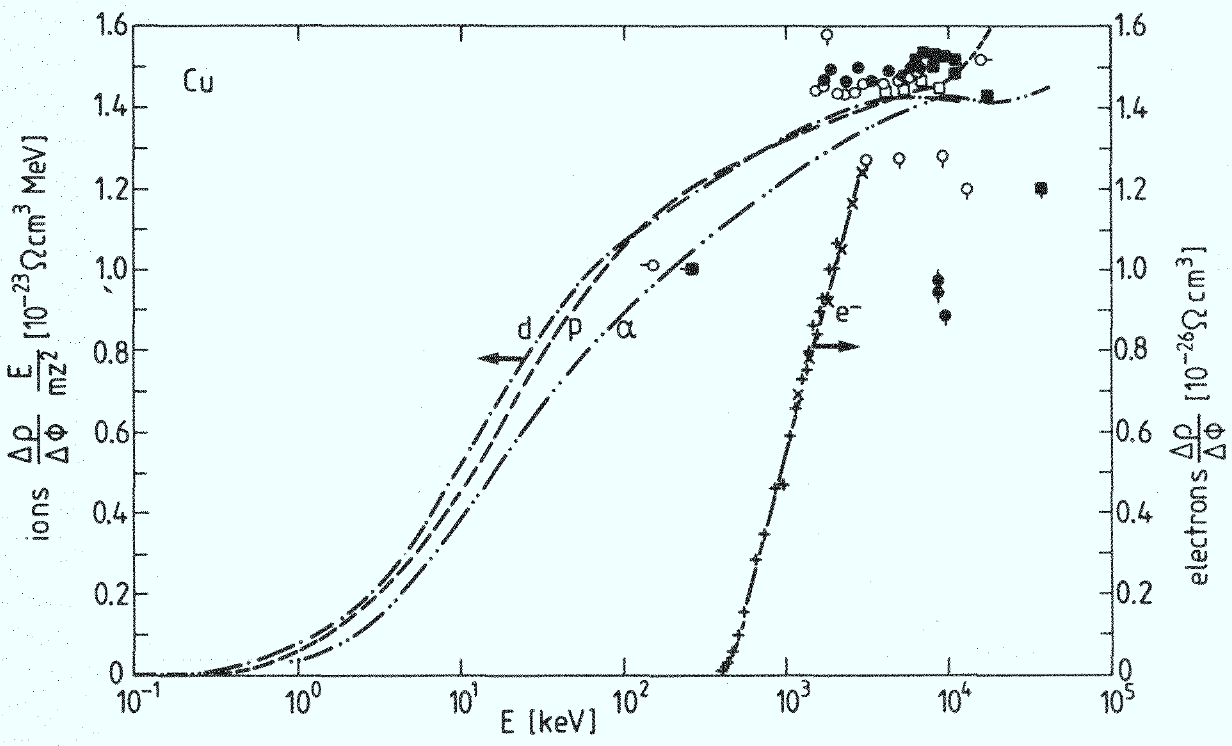

Fig. A4: Damage rates of electrons (+ Ref /50/, x Ref /58/) and normalized damage rates for protons (o Ref /4/, ♀ Ref /59/, -o Ref /28/, o- Ref /57/, deuterons (● Ref /4/, ● Ref /59/, ● Ref /60/, He^3 (□ Ref /4/), and α-particles (■ Ref /4/, ■ Ref /59/, -■ Ref /28/) in Cu as a function of energy. The curves are calculated for electrons (——), protons (--), deuterons (-·-) and α-particles (—··—).

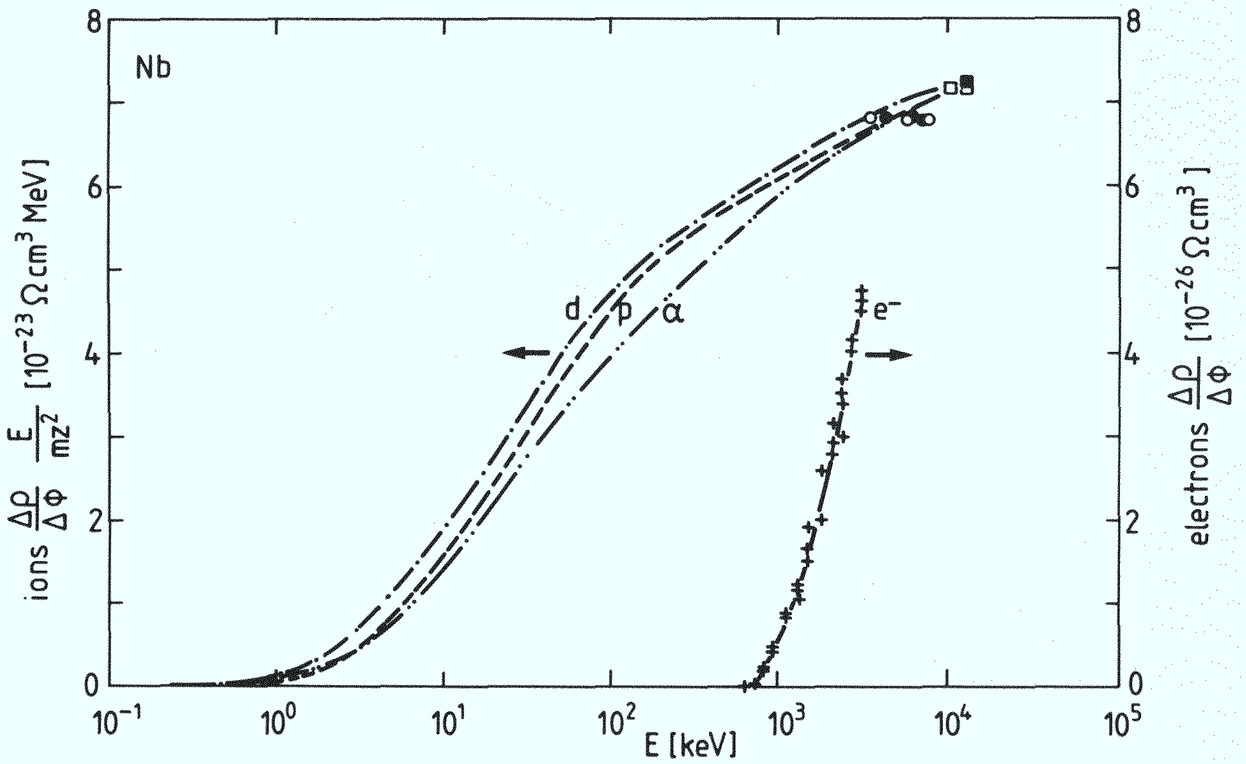

Fig. A5: Damage rates for electrons (+ Ref /54/) and normalized damage rates for protons (o), deuterons (●), He^3 (□) and α-particles (■) from Ref /4/ in Nb as a function of energy. The curves are calculated for electrons (——), protons (--), deuterons (-·-) and α-particles (--·· -).

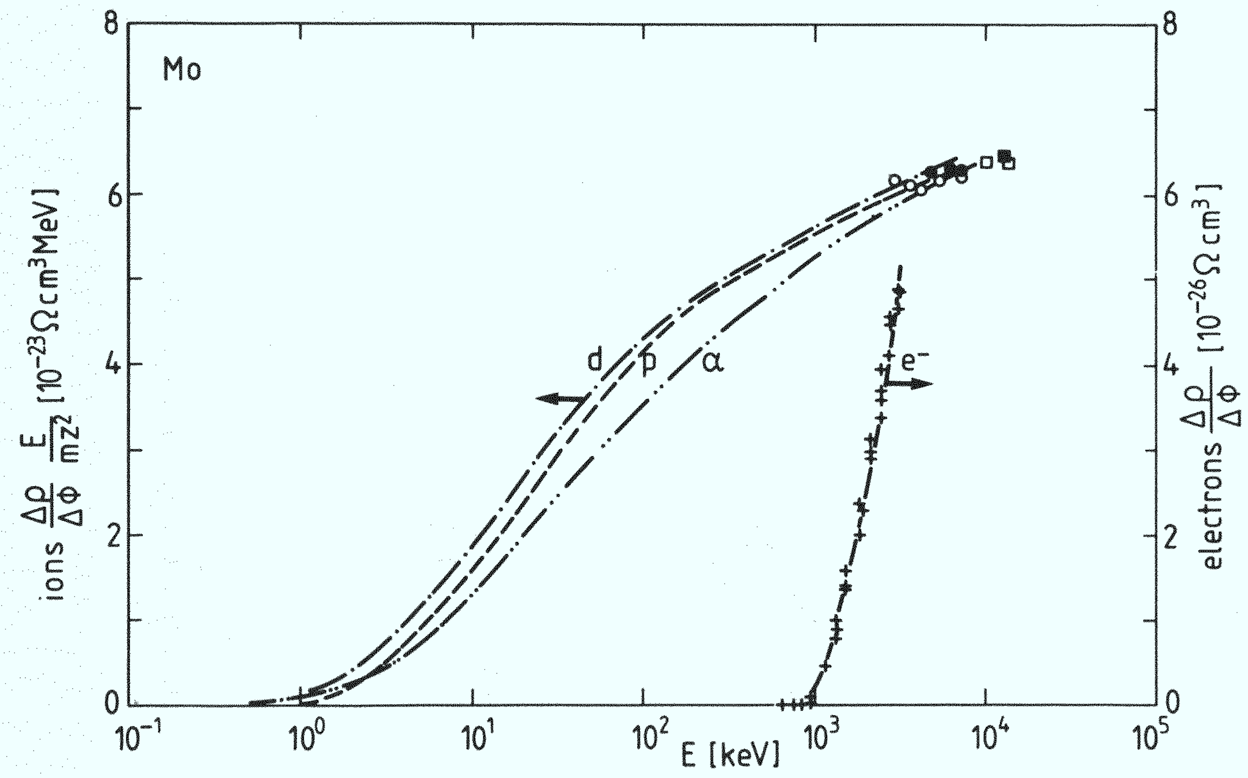

Fig. A6: Damage rates for electrons (+ Ref /54/) and normalized damage rates for protons (o), deuterons (•), He^3 (□) and α-particles (■) from Ref /4/ in Mo as a function of energy. The curves are calculated for electrons (—), protons (--), deuterons (-•-) and α-particles (--··-).

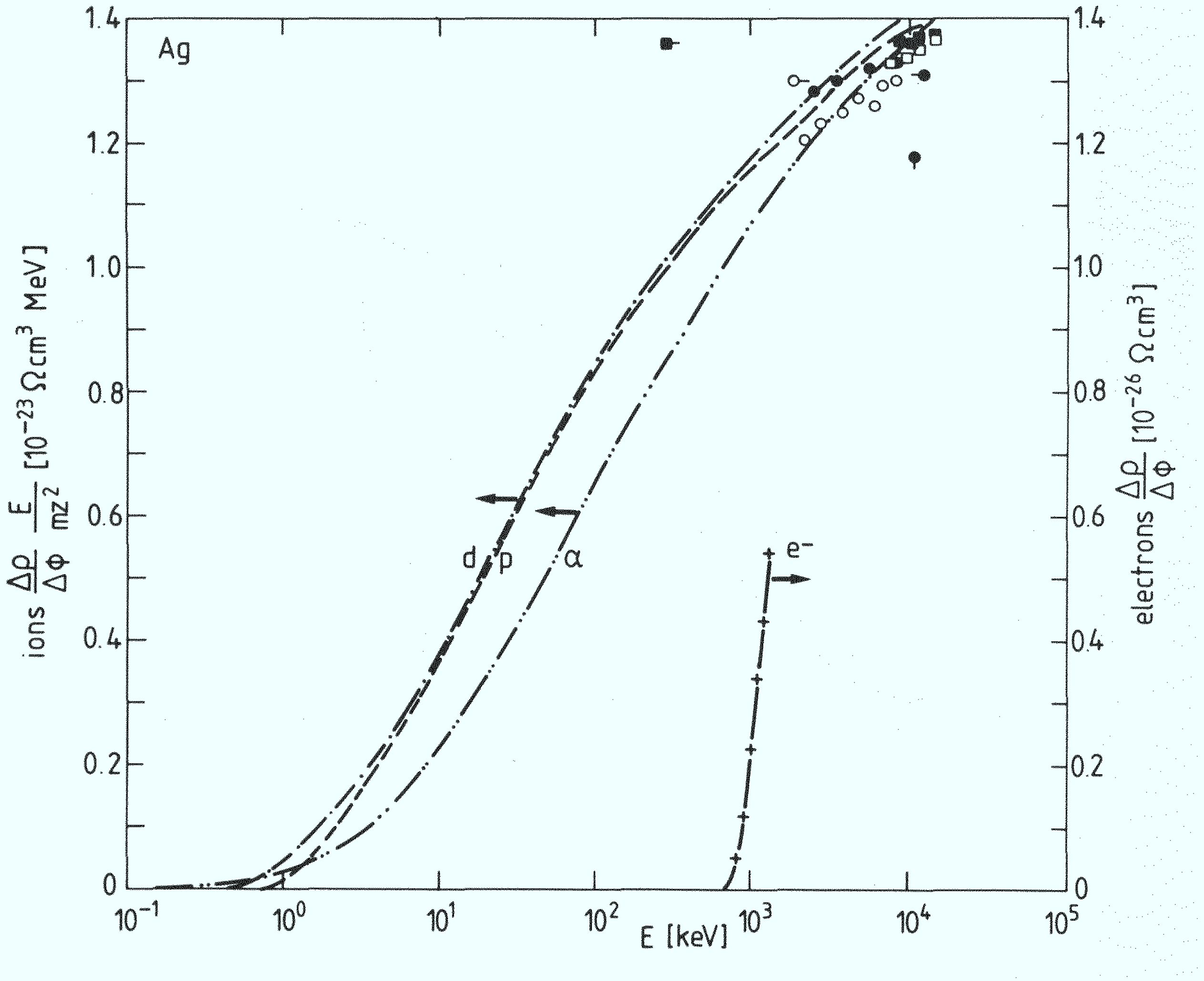

Fig. A7: Damage rates for electrons (+ Ref /56/) and normalized damage rates for protons (o Ref /4/, o– Ref /28/), deuterons (● Ref /4/, –● Ref /61/, ● Ref /60/), He^3 (□ Ref /4/) and α-particles (■ Ref /4/, ■– Ref /28/) in Ag as a function of energy. The curves are calculated for electrons (—), protons (--), deuterons (-·-) and α-particles (—··—).

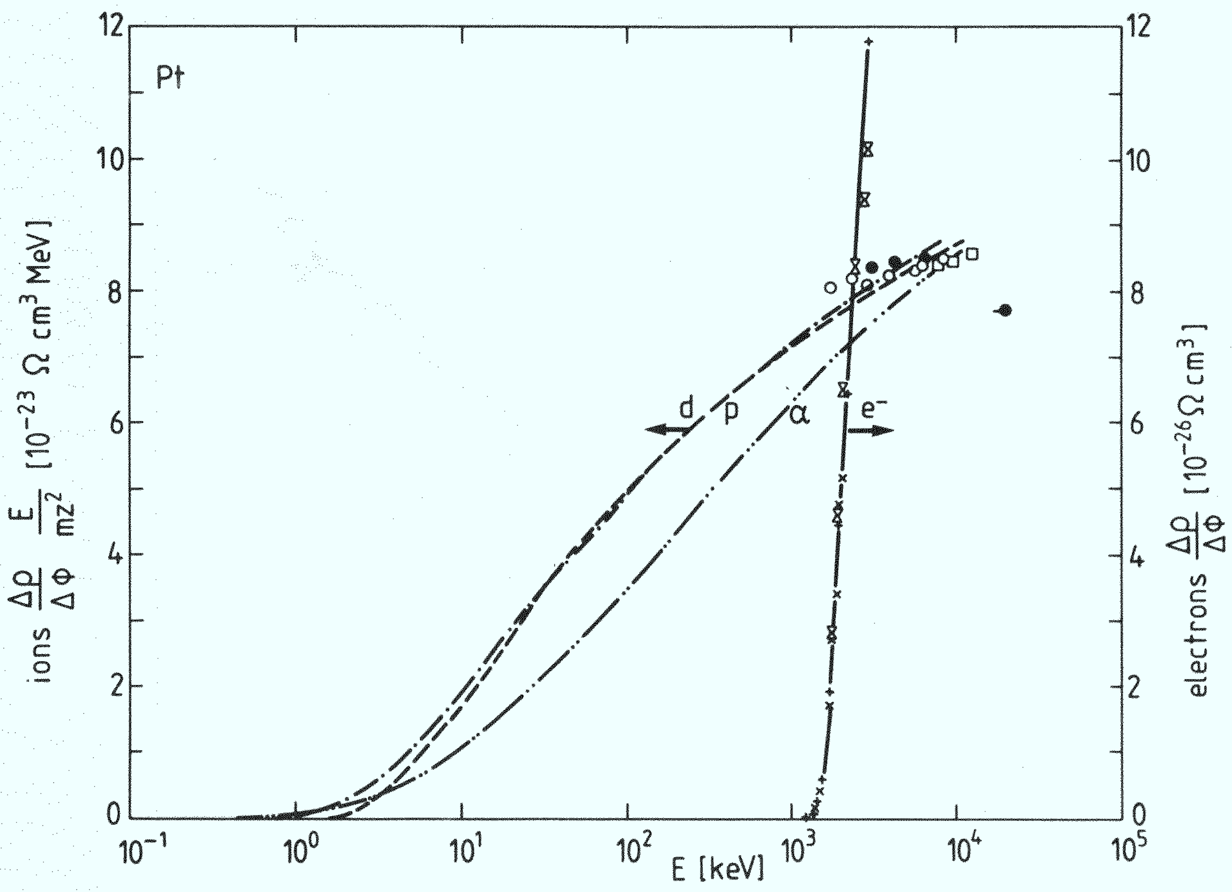

Fig. A8: Damage rates for electrons (+ Ref /62/, x Ref /63/, ⧗ Ref /64/) and normalized damage rates for protons (o Ref /4/) deuterons (● Ref /4/, -● Ref /52/) and He^3 (□ Ref /4/) in Pt as a function of energy. The curves are calculated for electrons (——), protons (--), deuterons (-·-) and α-particles (——··-).

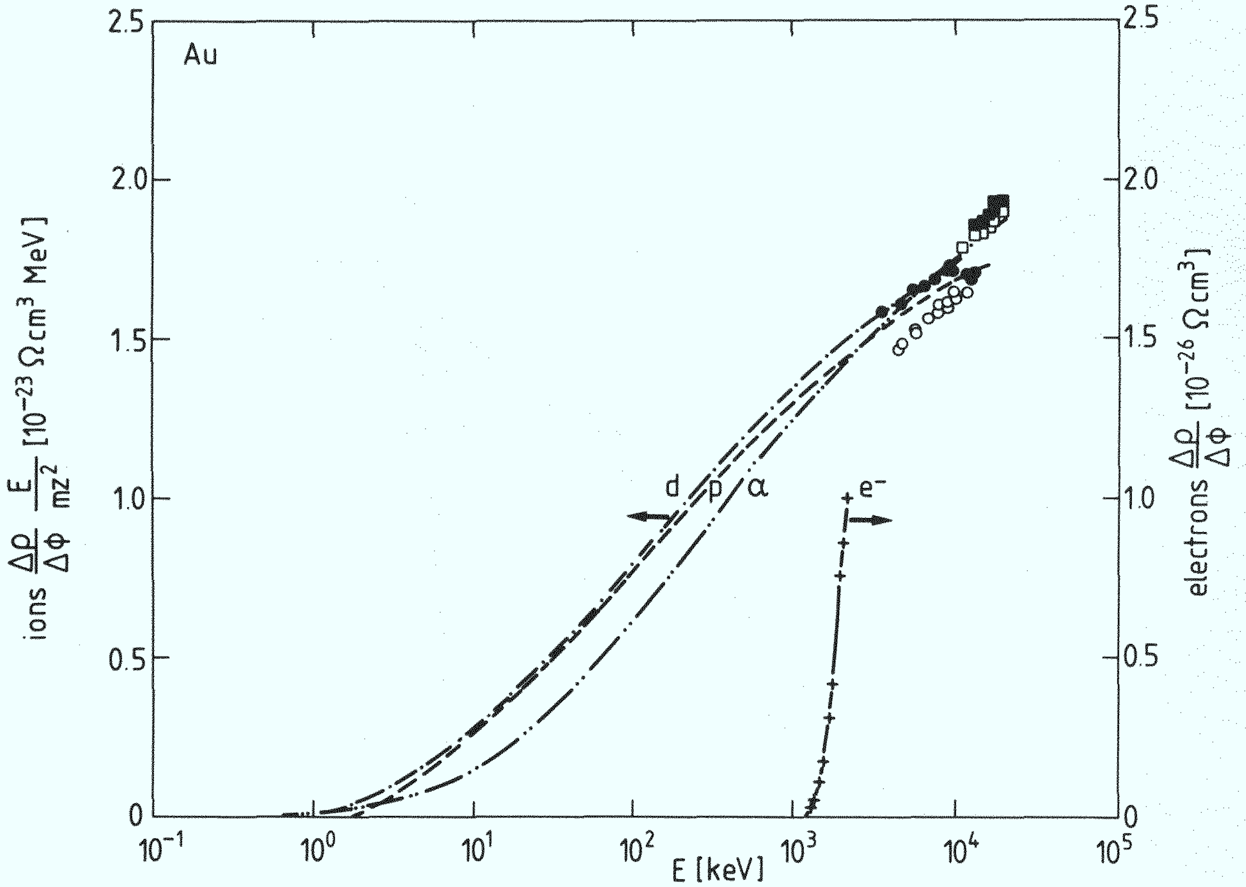

Fig. A9: Damage rates for electrons (+ Ref /65/) and normalized damage rates for protons (o Ref /4/), deuterons (● Ref /4/, ● Ref /52/), He^3 (□ Ref /4/) and α-particles (■ Ref /4/, ■ Ref /66/) in Au as a function of energy. The curves are calculated for electrons (——), protons (--), deuterons (-·-) and α-particles (—··-).

APPENDIX B

Cross sections for He production and He-to-dpa ratios under proton and deuteron irradiation.

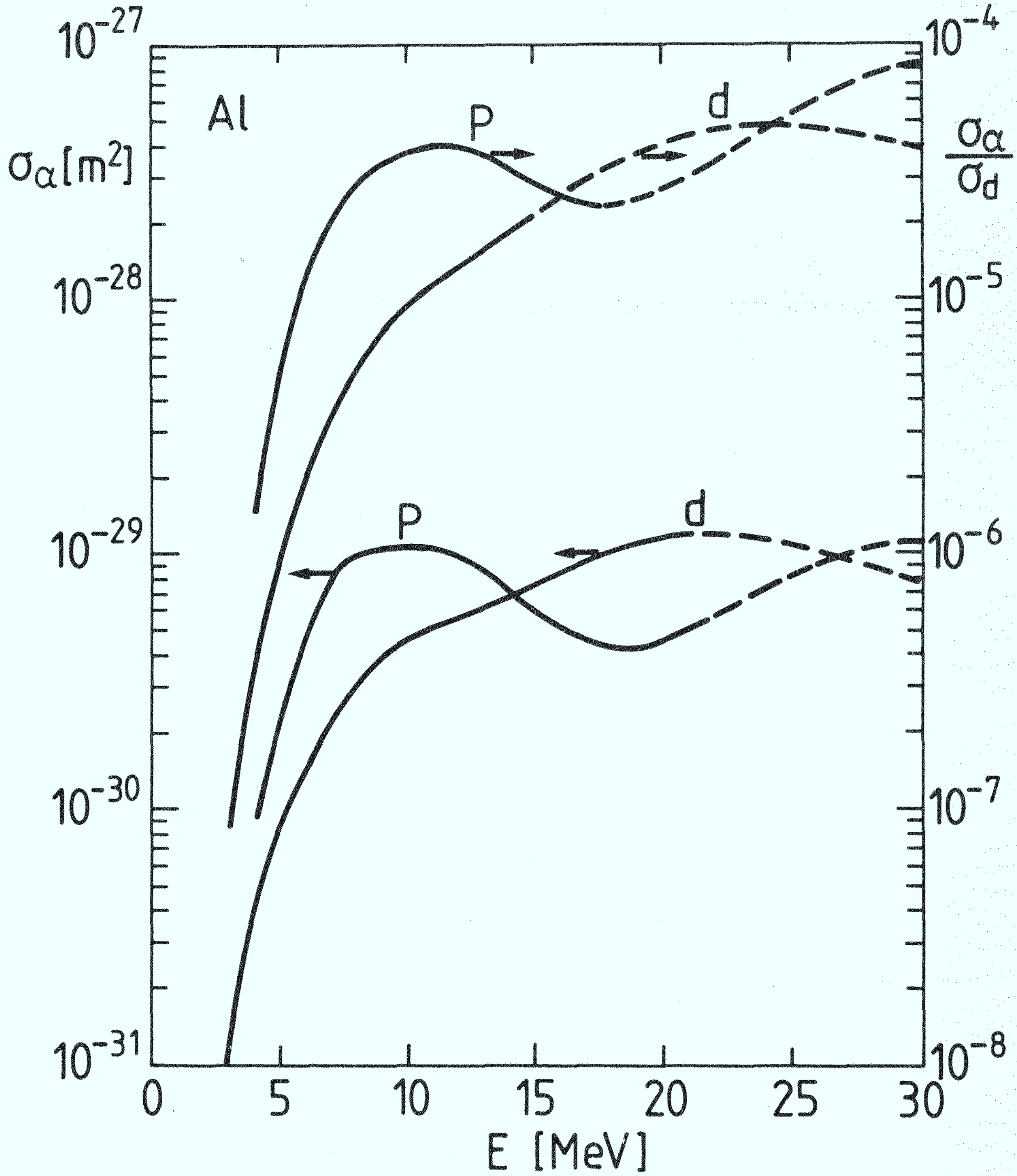

Fig. B1: Approximate cross section for the production of Helium in Al during p- and d-irradiation, respectively, as a function of energy. The cross sections include (p,α), (p,αn), (d,α) and (d,αn) reference functions from /40/ and experimental cross sections for (d,αp) as cited in /40/. The upper curves give He to dpa ratios using the displacement cross sections of Fig. A1. Dashed parts of the curves correspond to extrapolations of the σ_d- or σ_α-curves.

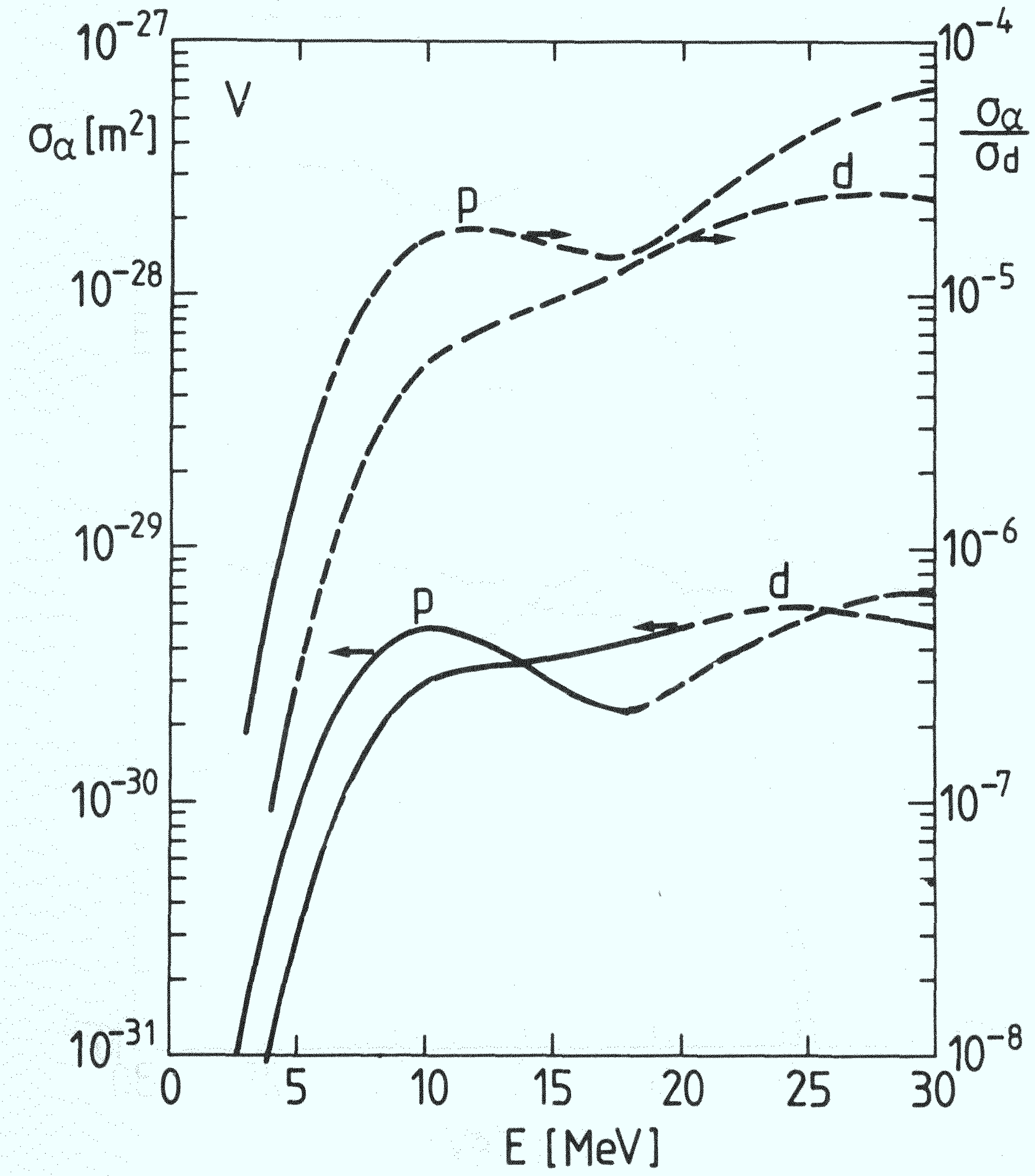

Fig. B2: Approximate cross sections for the production of Helium in V during p- and d-irradiation, respectively, as a function of energy. The cross sections include (p,α), (p,αn), (d,α) and (d,αn) reference functions from /40/ and experimental cross sections of ^{51}V (p,αp) as cited in /40/. The upper curves give He-to-dpa-ratios using the displacement cross sections of Fig. A2. Dashed parts of the curves correspond to extrapolations of the σ_d- or σ_α-curves.

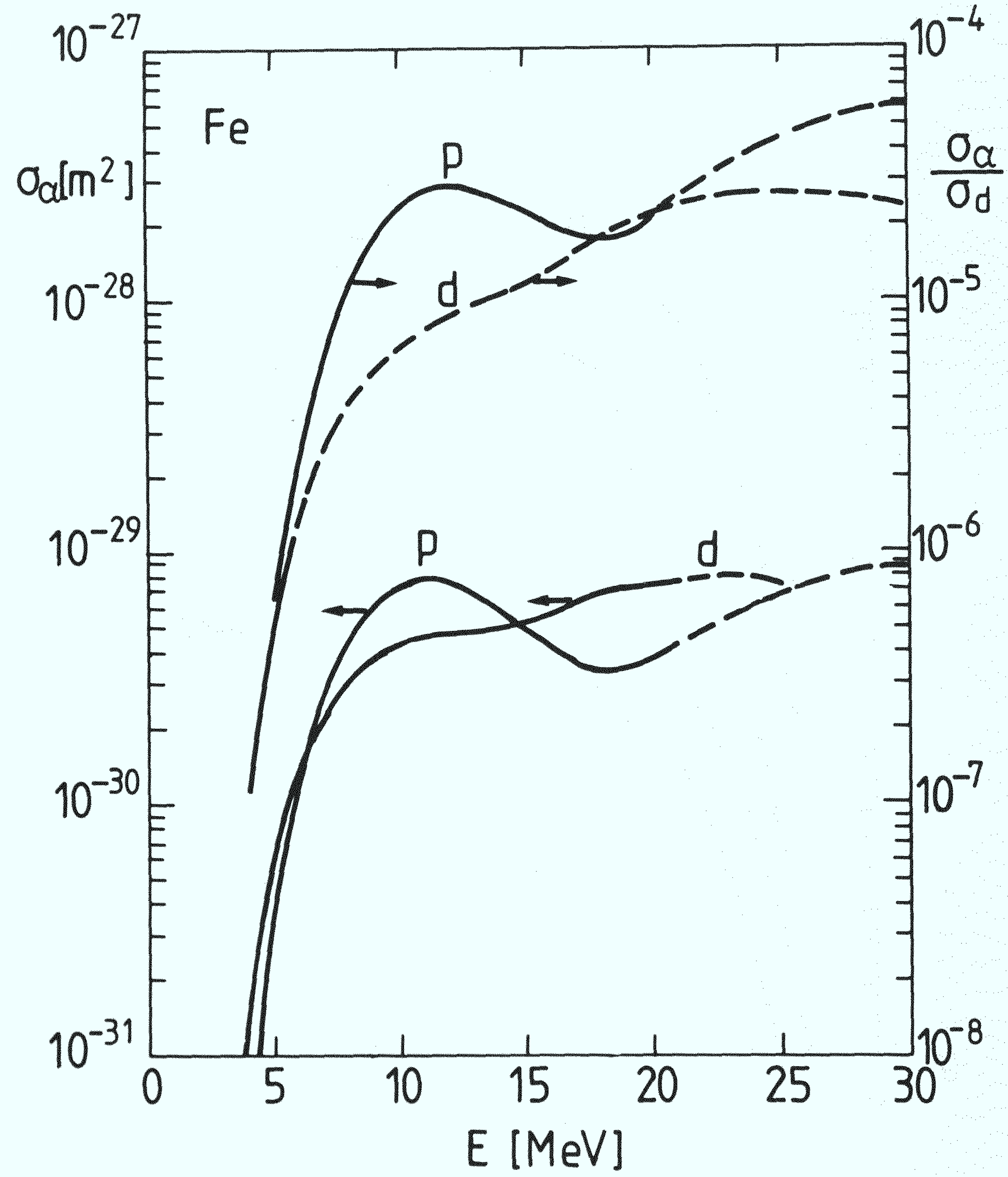

Fig. B3: Approximate cross sections for the production of Helium in Fe during p- and d-irradiation, respectively, as a function of energy. The cross sections include (p,α), (p,αn), (d,α) and (d,αn) reference functions from /40/. The (d,α) function is in reasonable agreement with experimental data for $^{54}Fe(d,\alpha)$ as cited in /40/. The upper curves give He-to-dpa-ratios using the displacement cross sections of Fig. A3. Dashed parts of the curves correspond to extrapolations of the σ_d- or σ_α-curves.

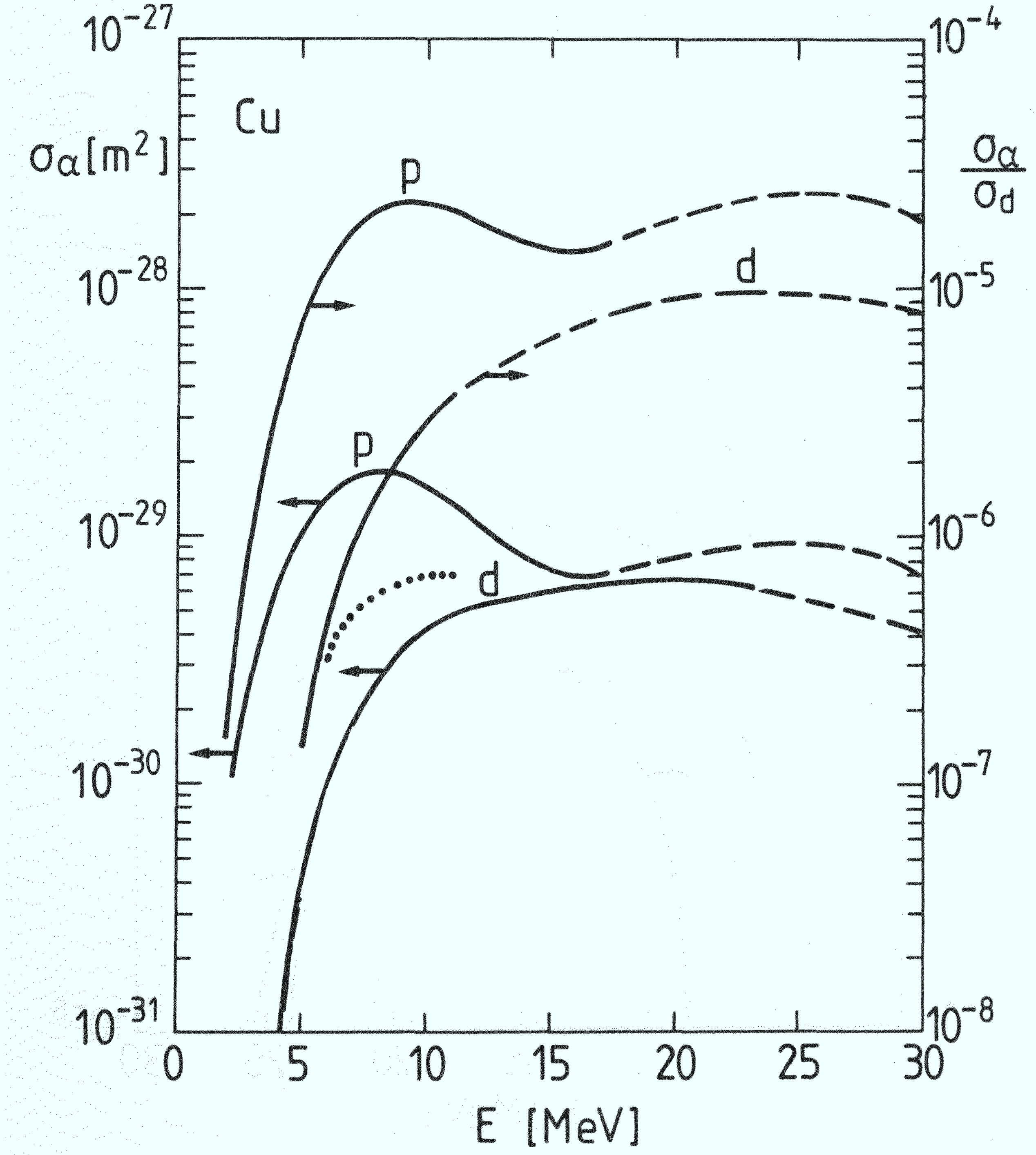

Fig. B4: Approximate cross sections for the production of Helium in Cu during p- and d-irradiation, respectively, as a function of energy. The cross sections include (p,α), (p,αn), (d,α) and (d,αn) reference functions from /40/. Experimental cross sections for $^{63}Cu(p,\alpha)$ as cited in /40/ (dotted line) cover only a narrow energy range. The upper curves give He to dpa ratios using the displacement cross sections of Fig. A4. Dashed parts of the curves correspond to extrapolations of the σ_d- or σ_α-curves.

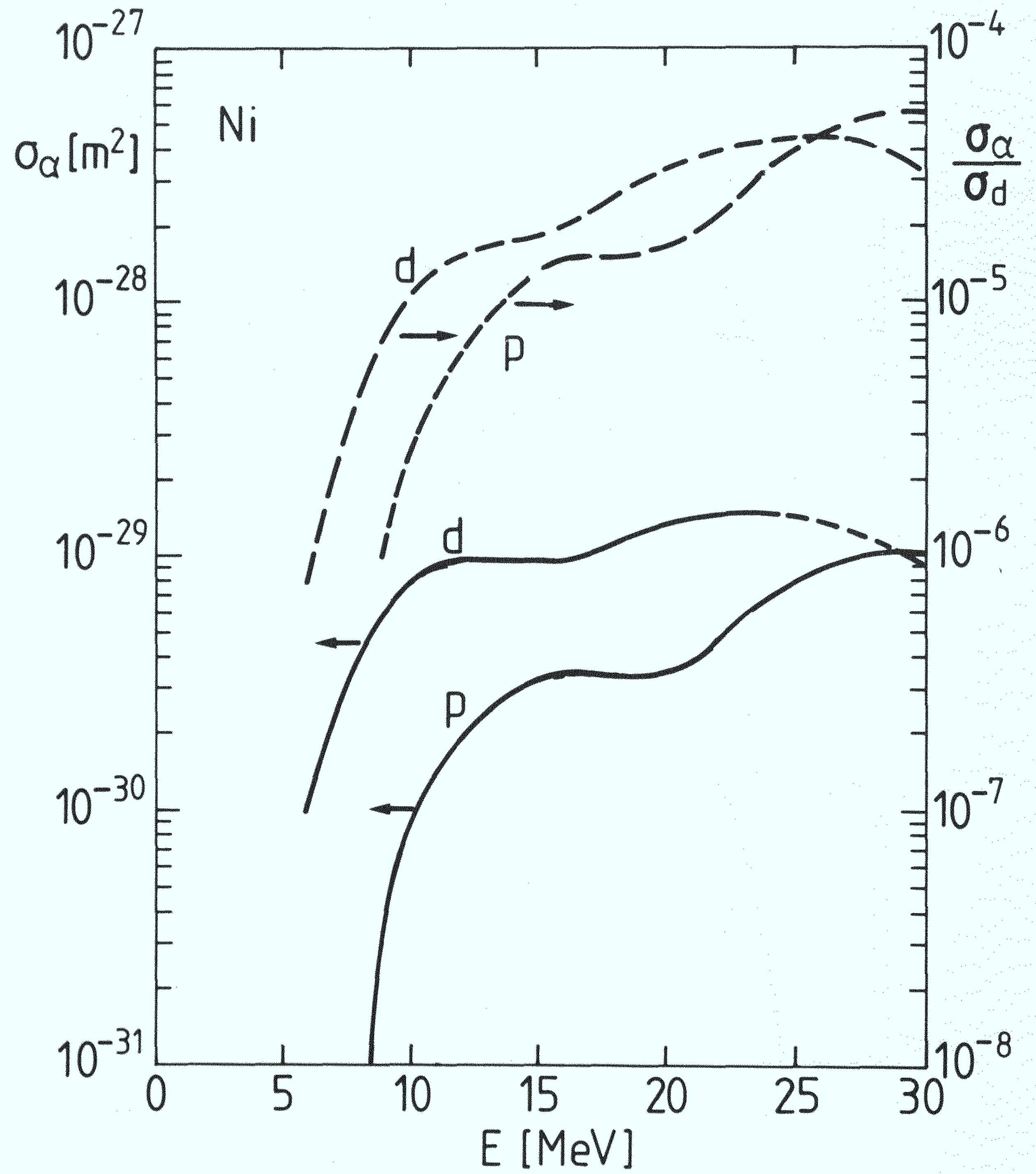

Fig. B5: Cross sections for the production of Helium in Ni during p- and d-irradiation, respectively, as a function of energy. The cross sections include experimental data of ^{58}Ni (p,α), ^{62}Ni (p,αn), ^{62}Ni (p,α2n), ^{58}Ni (d,α), ^{58}Ni (d,αn) and ^{58}Ni (d,α2n) reactions as cited in Ref /11/. The upper curves give He-to-dpa ratios using the displacement cross sections of table III.

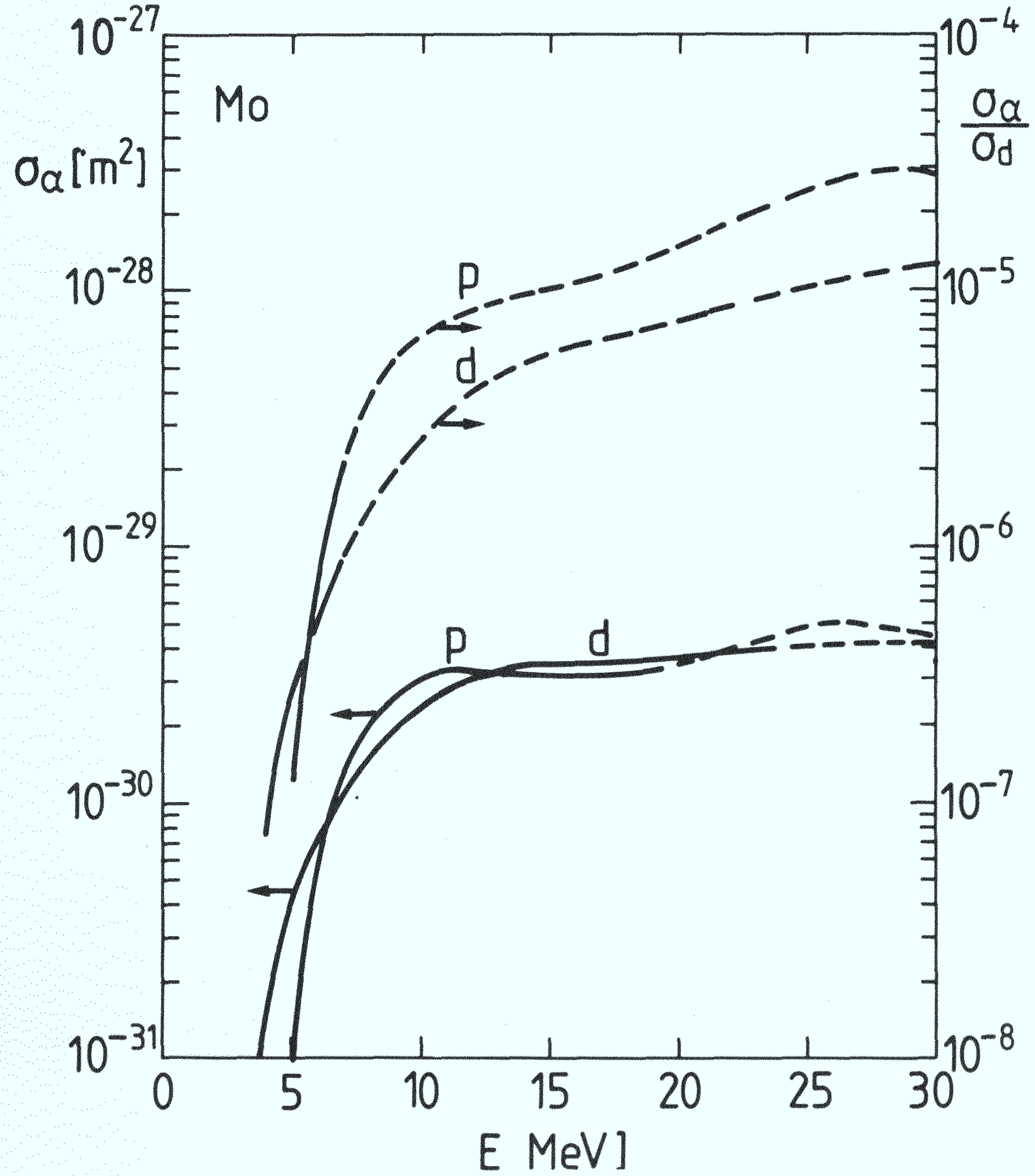

Fig. B6: Approximate cross sections for the production of Helium in Mo during p- and d-irradiation, respectively, as a function of energy. The cross sections include (p,α), (p,αn), (d,α) and (d,αn) reference functions from /40/. The upper curves give the to dpa ratios using the displacement cross sections of Fig. A6. Dashed parts of the curves correspond to extrapolations of the σ_d- or σ_α-curves.